Hindawi
Shock and Vibration
Volume 2018, Article ID 3740208, 21 pages
https://doi.org/10.1155/2018/3740208

Research Article

Assessment of the Magnetic Hysteretic Behaviour of MR Dampers through Sensorless Measurements

Janusz Gołdasz,[1,2] **Bogdan Sapinski**,[3] **and Łukasz Jastrzębski**[3]

[1]*Department of Automation and Information Technology, Cracow University of Technology, Kraków, Poland*
[2]*BWI Group, Technical Center Kraków, Kraków, Poland*
[3]*Department of Process Control, AGH University of Science and Technology, Kraków, Poland*

Correspondence should be addressed to Janusz Gołdasz; jgoldasz@pk.edu.pl

Received 5 January 2018; Accepted 15 July 2018; Published 9 September 2018

Academic Editor: Mario Terzo

Magnetorheological (MR) dampers are well-known devices based on smart fluids. The dampers exhibit nonlinear hysteretic behaviour which affects their performance in control systems. Hence, an effective control scheme must include a hysteresis compensator. The source of hysteresis in MR dampers is twofold. First, it is due to the compressibility and inertia of the fluid. Second, magnetic hysteresis is the inherent property of ferromagnetic materials that form the control circuit of the valve including MR fluid. While the former was studied extensively over the past years using various phenomenological models, the latter has attracted less attention. In this paper, we analyze the magnetic hysteretic behaviour of three different MR dampers by investigating their current-flux relationships. Two dampers operate in flow mode, whereas the third one is a shear-mode device (brake). The approach is demonstrated using a sensorless magnetic flux estimation technique. We reveal the response of the dampers when subjected to sinusoidal inputs across a wide range of operating conditions and excitation inputs. Our observations of the flux data showed that the hysteresis is influenced by both amplitude and the frequency of the excitation input. The procedure allows to analyze the magnetic hysteresis independently of other sources of hysteresis in MR dampers; on this basis, more effective damper models and control algorithms can be developed in the future.

1. Introduction

MR fluids are representatives of smart fluids. They are suspensions of microsize noncolloidal and low-coercivity particles in a nonconducting carrier fluid. When subjected to magnetic stimuli of sufficient strength, they develop a yield stress [1]. The unique feature in addition to high dynamic range, low hysteresis, low power consumption, temperature stability, and extremely fast response has made the material suitable for use in real-time applications of control systems. The technology has been commercialized by the automotive industry in semiactive vehicle chassis platforms (dampers) or powertrain mounts in particular [2, 3]. At the same time, the devices have revealed complex nonlinear characteristics due to the rheology of the fluid itself (shear rate versus shear rate behaviour, yield stress versus magnetic field characteristics) and inherent characteristics of the ferromagnetic materials (nonlinear flux density-field strength magnetisation curves, magnetic saturation) that constitute the magnetic circuit of the device. These contributors have translated into a nonlinear variation of the damper's force output with respect to the electromagnetic stimuli as well as the mechanical input (relative velocity/displacement). In a typical MR damper-based control system as shown in Figure 1, the information from the plant's onboard diagnostics, for example, vehicle's CAN bus, and sensors is processed through a control algorithm. Based on the data, the resulting current command i_{cmd} is computed and sent to the current driver. At a given time instant, the current command results in the input voltage supply u and the output coil current i_{c}. Given the displacement (velocity) (x (v)), the damper generates the output force F. Apart from meeting real-time requirements, there are several factors that make the process complicated: magnetic hysteresis, mechanical (hydraulic) hysteresis, temperature, friction, nonlinear relationship between current (flux) and yield stress, and so on.

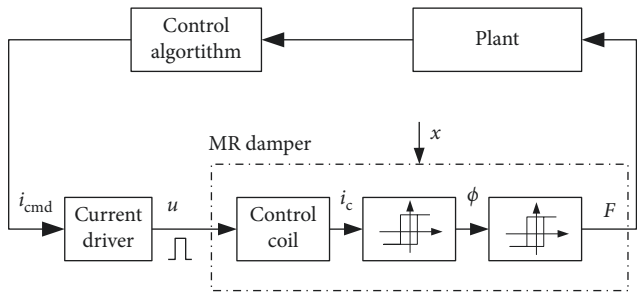

Figure 1: Block diagram of an MR damper-based vibration control system.

In the case of MR dampers, the source of hysteresis is twofold (mechanical/hydraulic and magnetic). First, the fluid itself is compressible. The influence of compressibility is then manifested, for example, as the hysteresis in force-velocity plots while stroking the damper. This can be related to the dynamics of a relatively heavy MR fluid mass being pushed through a long annular flow path whose resistance varies according to the flux-induced yield stress. The effect can be observed with or without the magnetic field applied, and it changes with the mechanical excitation frequency as thoroughly discussed in [4]. To summarize, the hydraulic hysteresis depends on the current amplitude applied and the mechanical input frequency. As the mechanical input frequency decreases, that hysteresis is also reduced. The hysteresis of magnetic materials that form the magnetic circuit of MR dampers (valves) is of more complex nature and its merits to be analyzed independently from the other sources.

The phenomenon of magnetic hysteresis is typical of any ferromagnetic material. Although certain fail-safe applications take advantage of high coercivity exhibited by specific materials (hard magnets), soft magnetic (low coercivity) alloys are used in solenoid cores for low energy loss. Carbonyl iron (common solid-phase material of MR fluids) suspensions exhibit virtually no hysteresis [5]; however, the hysteresis of specific ferromagnetic materials constituting the magnetic circuit of the dampers must be taken into account. Contrary to the mechanical hysteresis, the magnetic one does not disappear when the excitation frequency approaches zero, and it manifests itself, for example, as an additional friction force.

The problem of magnetic hysteresis is also typical in control systems featuring electromagnetic components such as solenoid actuators. The behaviour of such systems has been studied extensively in the past [6], and various hysteretic models have been developed to handle the hysteresis. For example, one popular approach is based on the Preisach model in which the hysteresis is a sum of elementary hysteresis loops [7]. Also, Jiles and Atherton provided the popular model of magnetic hysteresis (J-A) [8]. Its advantage over the other models is that the model parameters can be related to physical properties of ferromagnetic materials [9]. The model is suitable for both isotropic and anisotropic magnetic materials [10] and has been extended to incorporate the temperature dependence [11]. The model was modified to include the eddy currents impact on the hysteresis [12]. In another study [13], a first-order differential equation links the field strength H and the flux density B. The Coleman–Hodgdon model parameters can be identified from physical measurements of the major $B-H$ loops. Both Preisach and Coleman–Hodgdon models can be vectorized. The model of Tellinen [14] is a simple scalar approach for solving hysteresis problems, and it uses the limiting hysteresis loop from physical measurements of ferromagnetic materials.

The significance of having a good-quality hysteresis model had been recognized early in control studies of MR dampers, and the reader should refer to [15] for a review of suitable phenomenological models as well as [16, 17]. However, the majority of these studies neglected the magnetic hysteresis or it was not analyzed separately from other sources. In general, the mechanical hysteresis was considered by examining the relationship between force and velocity/position, whereas the field-dependent hysteresis was considered by investigating the hysteresis between current and force. There a few notable exceptions. For example, in [18] as well as [19], the Preisach model was applied to identify the hysteretic behaviour of an MR fluid. Next, the Preisach approach was used to develop a model of an MR clutch [20]. Also, the Coleman–Hodgdon model was used to analyze the magnetic circuit hysteresis of an MR (rotary) clutch [21]. The authors identified parameters of the model from physical measurements of various ferromagnetic materials used in the clutch assembly. In another study of an MR clutch, a simple hysteretic model was used [22, 23]. In the model, the hysteresis is modeled by means of a first-order ordinary differential equation linking B and H. The authors claimed the model fast enough to meet relevant criteria for use in real-time control systems. A finite-element model of an MR clutch incorporating the magnetic hysteresis was developed with the J-A model and including fluid dynamics and motion dynamics. Recently, in [24], the transient response of a flow-mode MR damper was examined using the inverse J-A model of magnetic hysteresis.

Briefly, the present study is experimental. It is an attempt to reproduce the magnetic hysteretic behaviour of several MR dampers, namely, flow-mode dampers and a rotary shear-mode damper (brake), respectively, through voltage and current measurements followed by offline integration to obtain magnetic flux. Aspects of this research should be useful for modeling studies and control system design.

The paper is organized as follows. First, we present the MR dampers and describe their electrical parameters and basic geometry. Then, we proceed to highlight the data acquisition system and the experiment details and discuss

the excitation input range. Following the discussion, we provide the readers with details on the flux estimation technique and then present the experimental results. Finally, we draw conclusions.

2. Dampers

Shortly, three different MR dampers were tested as shown in Figure 2. The first damper was a 2010 Audi Quattro MR vehicle damper (Figure 2(a)). The damper is a flow-mode device. The other two dampers were the RD-8040 small-stroke damper operating in the flow mode and the RD-2028 MR shear-mode brake, respectively. The small-stroke damper is presented in Figure 2(b), whereas the rotary brake is presented in Figure 2(c). In the paper, we refer to the automotive damper as MRD1. MRD2 is the small-stroke Lord Corp. damper and MRD3 is their rotary brake.

MRD1 is a long-stroke damper whose coil resistance is approximately 1 Ω at ambient temperature. The device can be operated up to 5 A continuous current for 30 s. The piston rod diameter is 12.4 mm, and the inner cylinder tube is 46 mm. It is a pressurized monotube shock absorber.

MRD2 is also a monotube gas charged damper. Its current range is from 0 to 1 A continuous current (for 30 s), and the coil resistance including connecting cables is 4.4 Ω. For the remaining details, the reader should refer to the hardware's specification [25].

For comparison, MRD3 is a 5 Nm compact brake [26]. The device can be operated up to 1 A continuous current, and its coil resistance is 8.9 Ω. Other details of the dampers, for example, core and coil dimensions, coil turns, and the like, control valve geometries are unknown.

For each damper, we measured their current response to (open loop/uncontrolled) voltage step inputs using the test setup described in the sections below. The (uncontrolled) MRD1 response is shown in Figure 2(a). The current output of MRD2 is revealed in Figure 2(b) and that of MRD3 in Figure 2(c). Moreover, Table 1 contains the summary of response times for the MRD1 damper. Table 2 reveals the same metrics of the MRD2 damper, whereas Table 3 contains the response time summary of the rotary brake MRD3. By definition, the response time t_{63} is the time that takes the current to reach 63% of the steady-state level. Similarly, the times t_{90} and t_{95} indicate the current metrics to achieve 90% and 95% of the steady-state value in the ON state, respectively. Finally, the response times t_{37} and t_{10} and t_{05} indicate the time needed by the current to drop below 37%, 10%, and 5% of the steady-state value. The metrics vary with the step voltage input level. For example, in the case of the damper MRD1, the time t_{90} decreases from the initial 62 ms at 1 A down to 35 ms at 5 A. The MRD2 response times are similar to those of MRD1, whereas inspecting the response time summary of MRD3 shows numbers exceeding 200 ms.

Based on the brief review of the step response data and the measured coil circuit parameters, we expected the dampers to show distinct dynamic behaviour to be demonstrated in the following sections of this study.

3. Test Inputs and Configuration

In this section, we reveal the test rig configuration and sensor details and excitation inputs and then discuss the experiment.

The data acquisition (DAQ) system is illustrated in Figure 3. As shown in the figure, the measurement circuit incorporated a voltage supply, a power driver, and a PC computer with the InTeCo's RT-DAC 4 PCI AD/DA board [27] also running a MATLAB/Simulink model of the measurement system. The power driver's output current is 7 A max. The AD/DA board's sampling frequency was 1 kHz during the experiments. The measurement system allowed for the acquisition of the supply voltage $u(t)$, the induced coil voltage $u_c(t)$, and the current response $i_c(t)$ simultaneously.

All dampers were subjected to similar treatment and measurements. In each case, the experiment was split into two sections. In the first part of the test, we measured the behaviour of the dampers when subjected to sinusoidal voltage waveforms of time-varying amplitude: $u(t) = At\sin(2\pi ft)$, where A is the amplitude increase/decrease rate in V/s and f refers to frequency. In the second part of the test, we examined the response of the dampers to constant amplitude sinusoidal inputs of voltage. In this experiment series, we varied the voltage input frequency from 1 Hz to 25 Hz in 1 Hz increments: $u(t) = U\sin(2\pi ft)$.

In the case of the damper MRD1, the input voltage $u(t)$ was adjusted in such a way to result in peak current levels from 0 to 5 A in 1 A steps. With the damper MRD2, we varied the supply voltage up to 4.4 V, which resulted in peak current 1 A max. In the case of MRD3, the peak voltage was 8.9 V, again resulting in the maximum current level of 1 A. All dampers were air-cooled in an effort to maintain constant temperature.

4. Flux Estimation

The experiments required implementing a flux estimation procedure that is based on voltage and current measurements. The flux ϕ is relatively straightforward to be measured directly. Hall probes or magnetostrictive sensors can measure it in the magnetic structures provided there is access to the location of interest, for example, air gap of sufficient size. Alternatively, sensing coils can be employed for the same task (see [28] and [29] as well as [30] or [31]). In this scenario, since there is no physical access to the control valve(s), the flux is estimated from voltage and current measurements via offline integration as highlighted in Figure 4.

Let us then consider the simplest nonlinear lumped parameters model of one coil MR damper as shown in Figure 5. The model includes the input voltage source $u(t)$, the coil resistance R, and the nonlinear inductance $L(i)$. The model equation is then as follows:

$$u(t) = i_c(t)R + \frac{d\lambda}{dt}, \tag{1}$$

where $u(t)$ is the supply voltage and $\lambda(t) = N\phi$ is flux linkage, ϕ is the magnetic flux, N is coil wire turns, and $u_c(t) = d\lambda/dt$ is the induced coil voltage. By transforming and integrating (1), we get

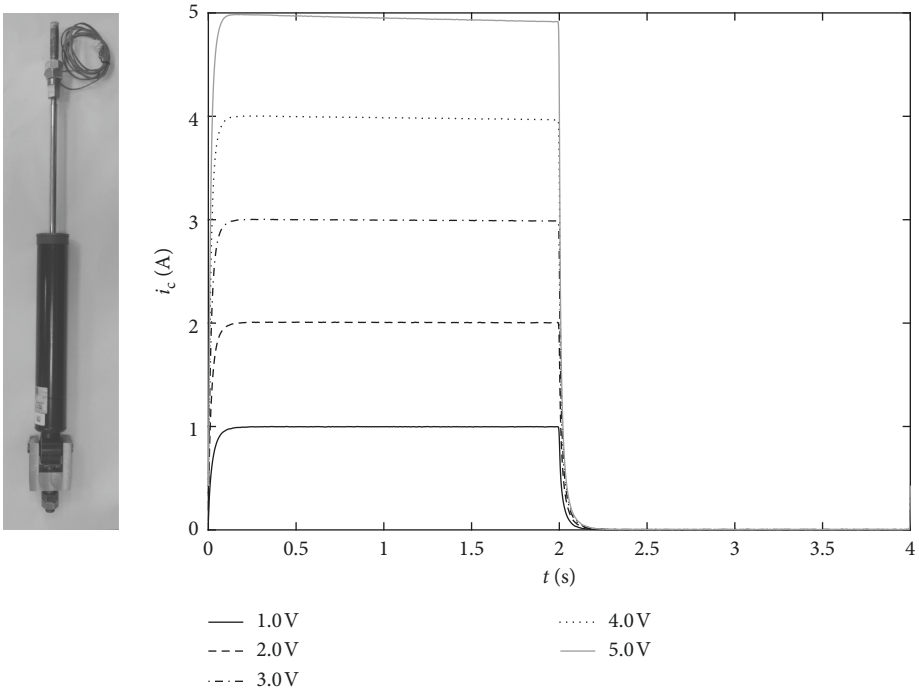

(a)

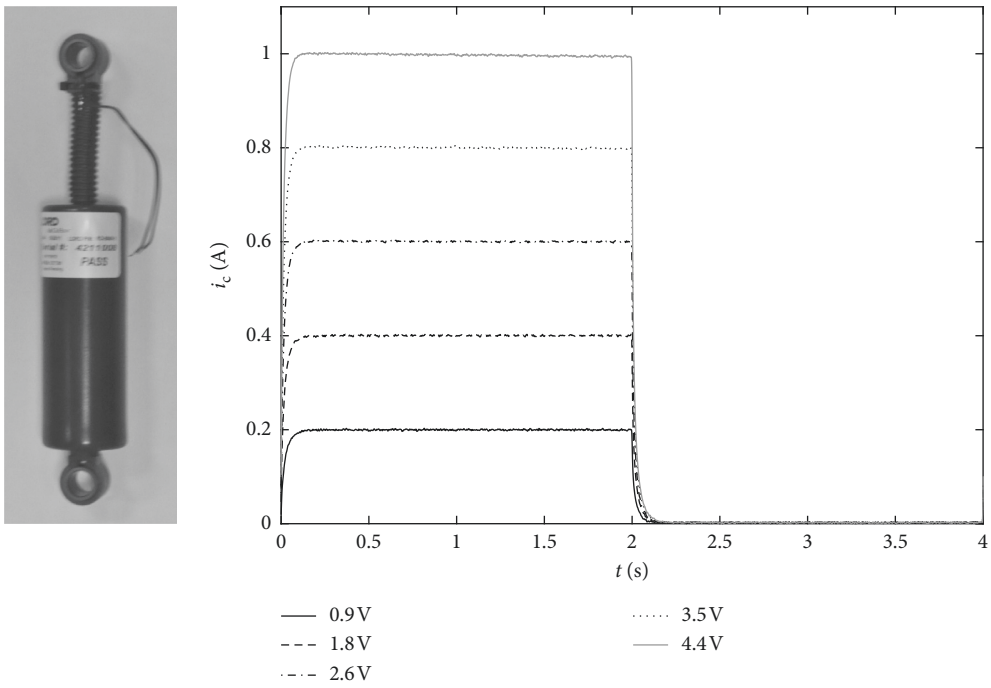

(b)

Figure 2: Continued.

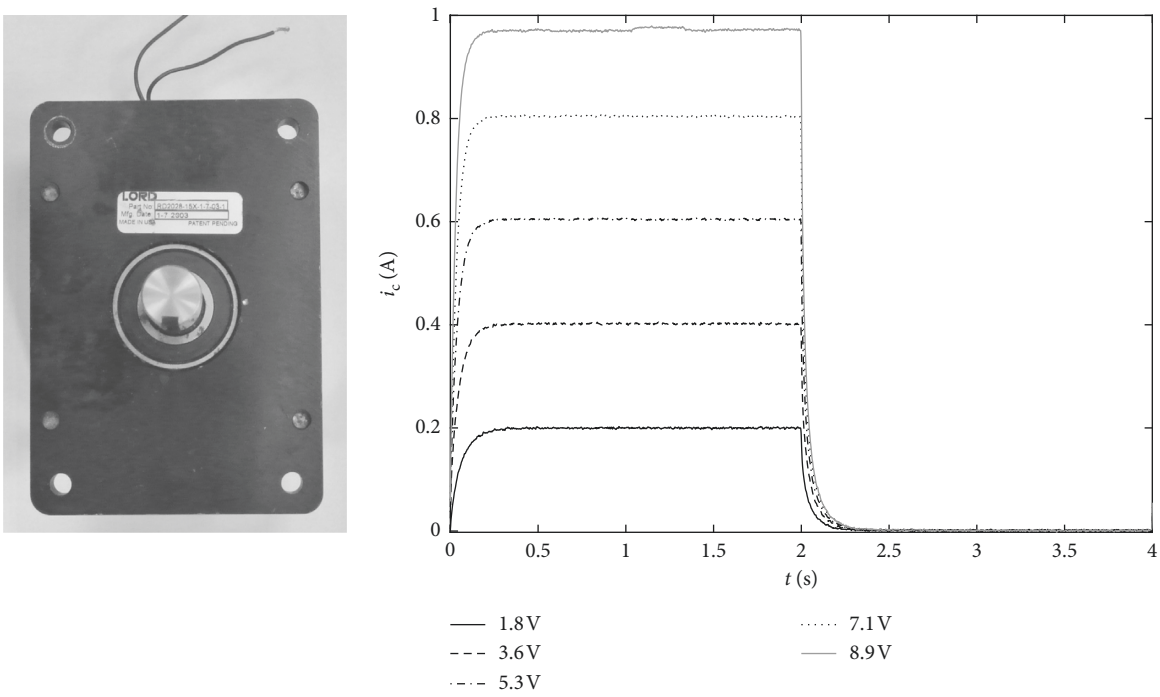

(c)

Figure 2: Images and (uncontrolled) response of the examined dampers. (a) MDR1. (b). MDR2. (c) MDR3.

Table 1: MRD1: response time summary.

I (A)	t_{63} (ms)	t_{90} (ms)	t_{95} (ms)	t_{37} (ms)	t_{10} (ms)	t_{05} (ms)
1	22	62	88	22	61	86
2	18	51	73	21	58	83
3	16	44	62	20	53	78
4	15	39	55	18	49	73
5	14	35	48	17	46	68

Table 2: MRD2: response time summary.

I (A)	t_{63} (ms)	t_{90} (ms)	t_{95} (ms)	t_{37} (ms)	t_{10} (ms)	t_{05} (ms)
0.2	20	65	93	19	56	70
0.4	17	51	73	19	55	79
0.6	15	45	65	19	48	69
0.8	14	42	59	18	49	72
1.0	13	38	52	17	46	67

Table 3: MRD3: response time summary.

I (A)	t_{63} (ms)	t_{90} (ms)	t_{95} (ms)	t_{37} (ms)	t_{10} (ms)	t_{05} (ms)
0.2	59	152	219	37	118	164
0.4	42	116	157	35	114	159
0.6	37	95	125	33	103	152
0.8	35	85	113	30	95	147
1.0	30	73	99	29	89	135

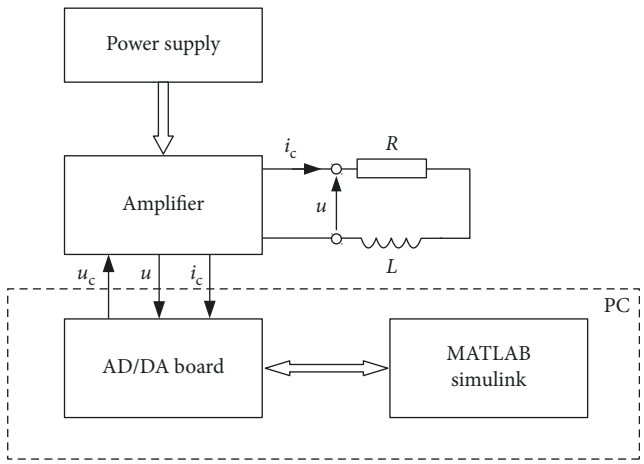

Figure 3: Data acquisition system layout.

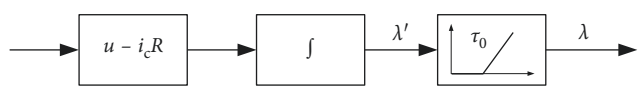

Figure 4: Experimental data processing layout; λ': (unfiltered) flux linkage, τ_0: high-pass filter time constant.

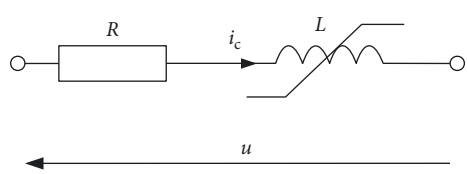

Figure 5: Equivalent control coil circuit.

$$\lambda(t) = N\phi(t) = \int_0^t \left(u(t) - i_c(t)R\right) dt. \quad (2)$$

The approach is common in control systems for solenoid actuators as well as motor drives [32]. Two major problems associated with this method are the measurement of coil resistance and the implementation of a good quality flux integrator [28]. While the coil resistance estimate can be rather easily obtained, the flux integrator is not trivial due to the resulting DC bias and drift due to measurement noise. Also, the unknown initial flux value is a problem that needs to be coped with, too.

To handle this scenario, several sensorless solutions have been proposed in the past for induction motors [33–35]. The authors proposed modified integrators or model-based compensation due to the drift. To reduce the DC offset and low-frequency fluctuations that were present in the measured data, we simply employed a high-pass filter as seen in Figure 4.

5. Experimental Results

In the sections that follow below, we reveal result of the experiment involving all three dampers. Each damper was examined at frequencies up to 25 Hz, namely, $f = \{1, 2, 3, 4, 5, 6, 8, 10, 15, 20, 25\}$ Hz. For the sake of brevity, we show only the 1, 5, 10, 25 Hz data, respectively. The frequency of the constant amplitude rate signal was 1 Hz. The signal's amplitude change rates were 1 V/s (MRD1), 0.4 V/s (MRD2), and 0.8 V/s (MRD3), respectively.

5.1. Results: MRD1. The results involving the vehicle suspension damper are illustrated in Figures 6–12. Specifically, Figures 6–7 reveal the data obtained by exciting the damper with the nonstationary amplitude voltage input. Figure 6 shows the measured time history of the coil current and the flux.

In Figure 7, the dataset was split into two 5 s sections each in order to highlight the damper's output during current rise and current decay phases, respectively. The figure illustrates the plots of current versus voltage and flux linkage versus current. Next, Figures 8–11 show the damper's output when subjected to (voltage) constant amplitude sinusoidal excitation inputs. As already mentioned, the input voltage amplitude was altered in such a way to result in the maximum amplitude of the coil current equal to 5 A at the initial frequency of 1 Hz. Finally, several steady-state characteristics are presented in Figure 12.

Observations of the plots show that increasing the frequency of the input voltage signal resulted in the current

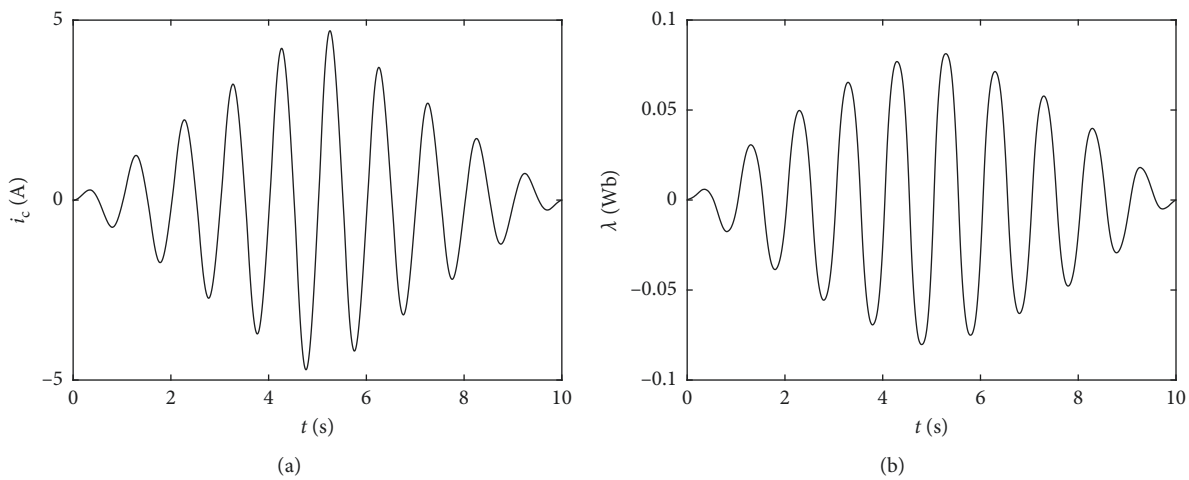

Figure 6: MRD1: time history of (a) current and (b) flux linkage.

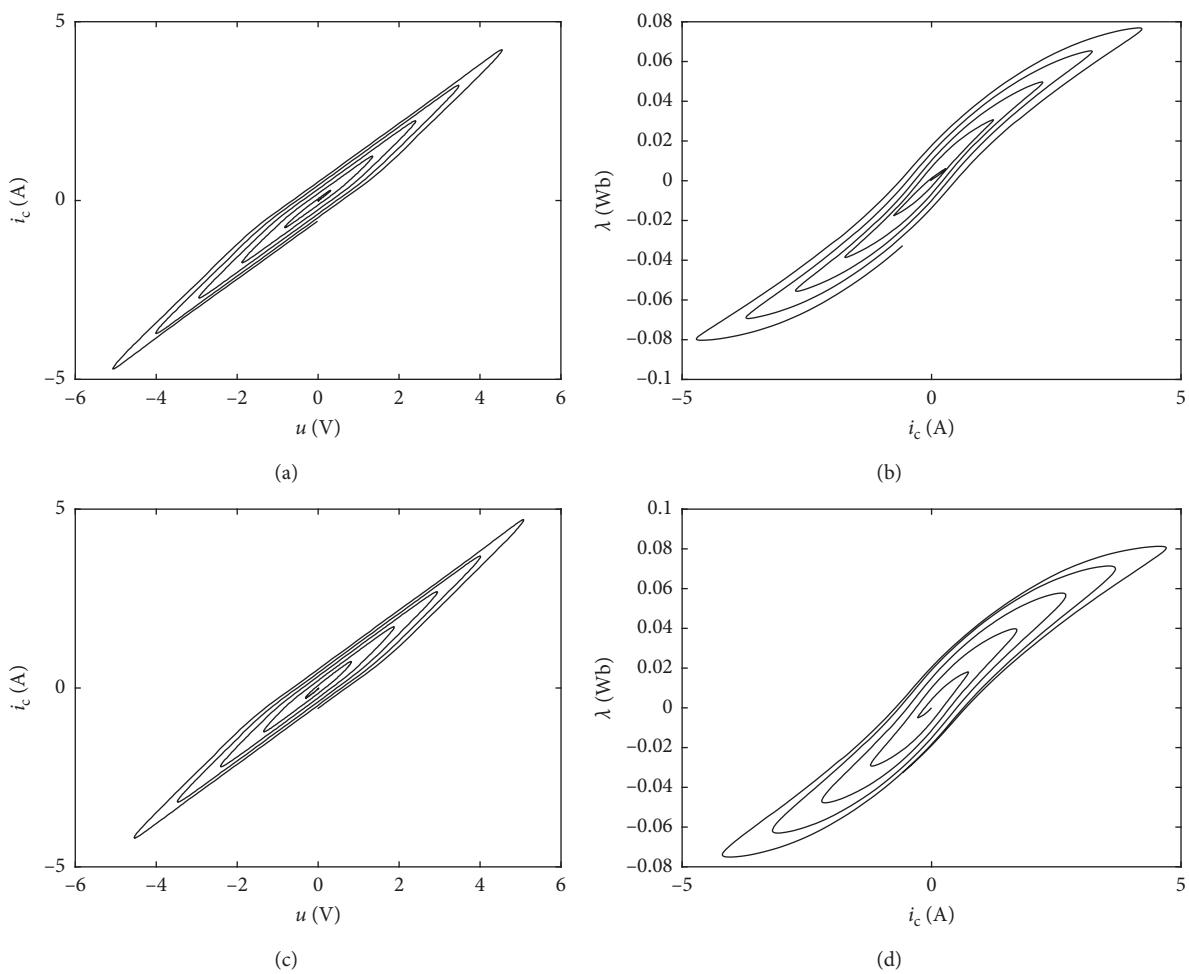

Figure 7: MRD1: (a, c) current versus voltage and (b, d) flux linkage versus current plots.

amplitude drop, for example, from the initial 5 A at $f = 1$ Hz down to approximately 2 A at $f = 25$ Hz. This was accompanied by the peak flux linkage Λ from the maximum 0.08 Wb ($f = 1$ Hz) to 0.02 Wb ($f = 25$ Hz) for approximately the same voltage input amplitude. Moreover, two other important aspects can be deduced from the plots. First, the hysteresis loop width grows with the input current applied. Second, the presence of hysteresis results in the variation of the magnetic flux linkage signal when increasing and decreasing the coil current.

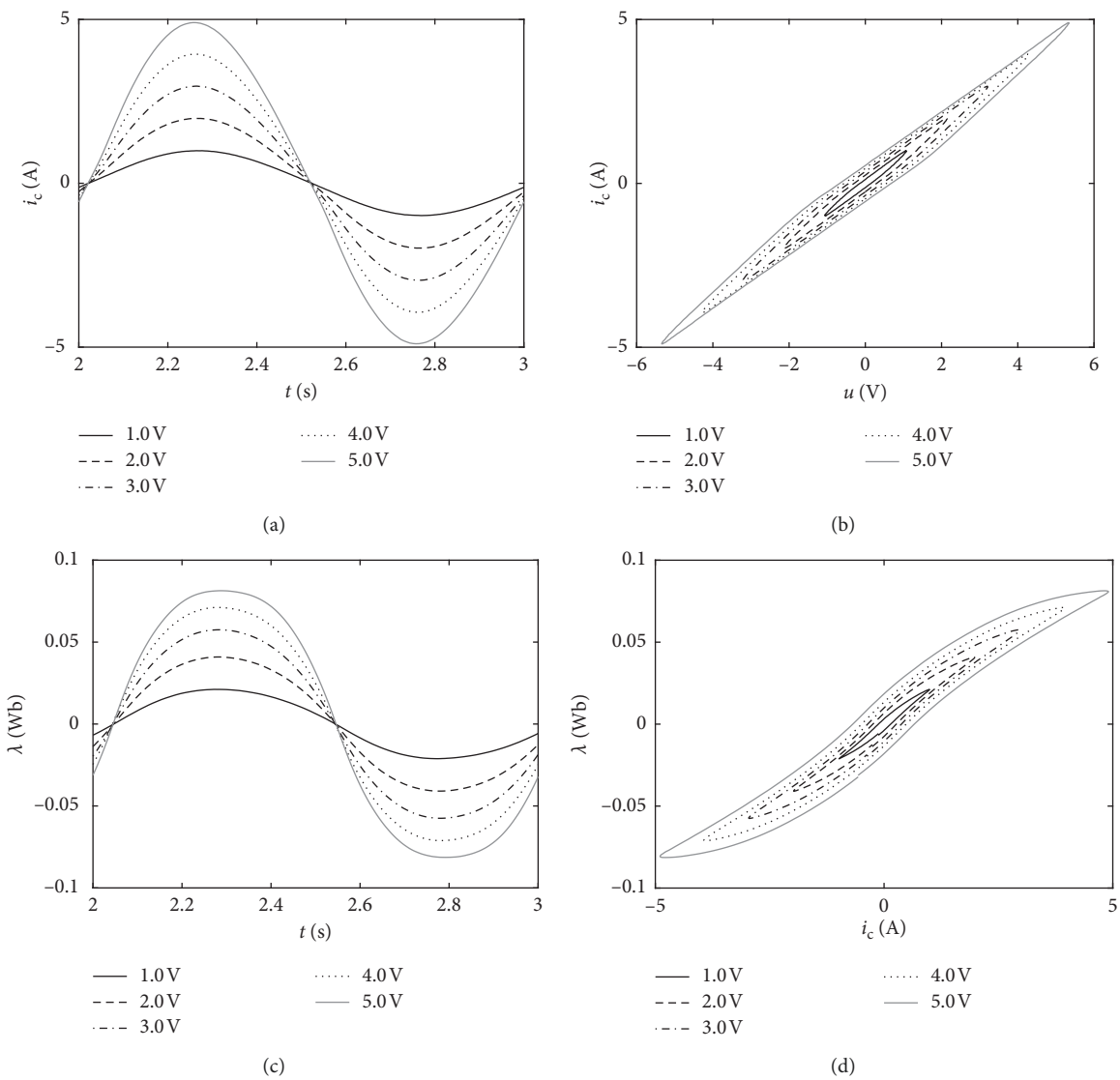

Figure 8: MRD1: sinusoidal input, $f = 1$ Hz. (a) i_c vs t, (b) i_c vs u, (c) λ vs t, and (d) λ vs i_c.

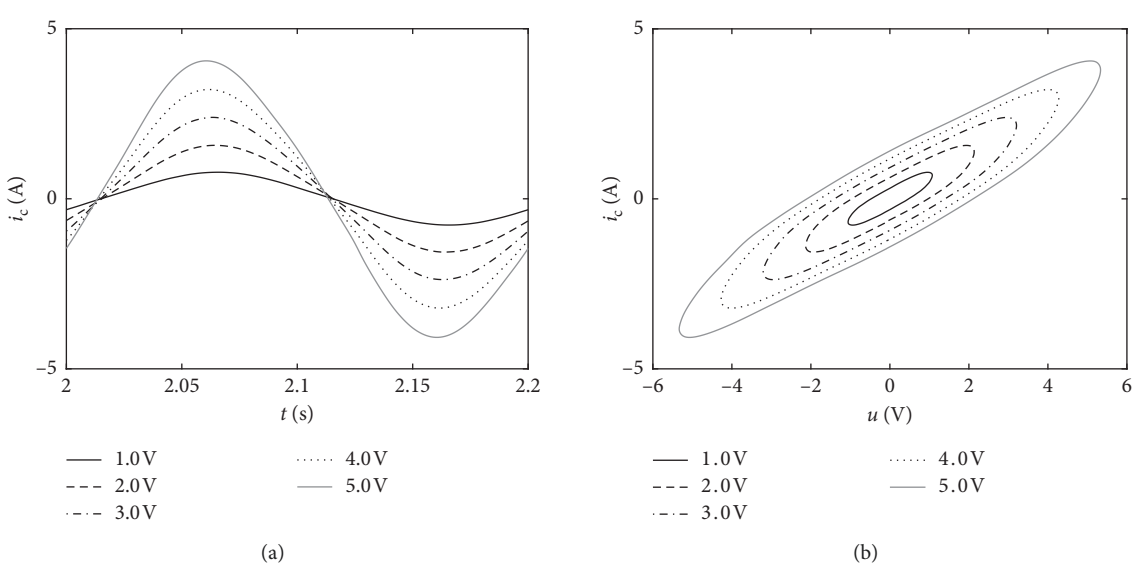

Figure 9: Continued.

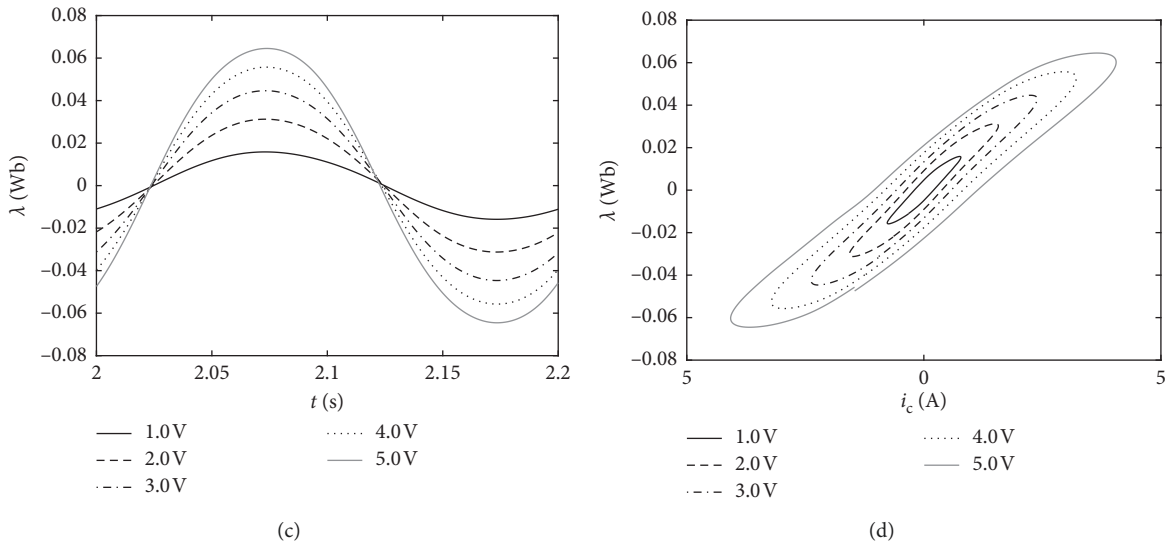

Figure 9: MRD1: sinusoidal input, $f = 5$ Hz. (a) i_c vs t, (b) i_c vs u, (c) λ vs t, and (d) λ vs i_c.

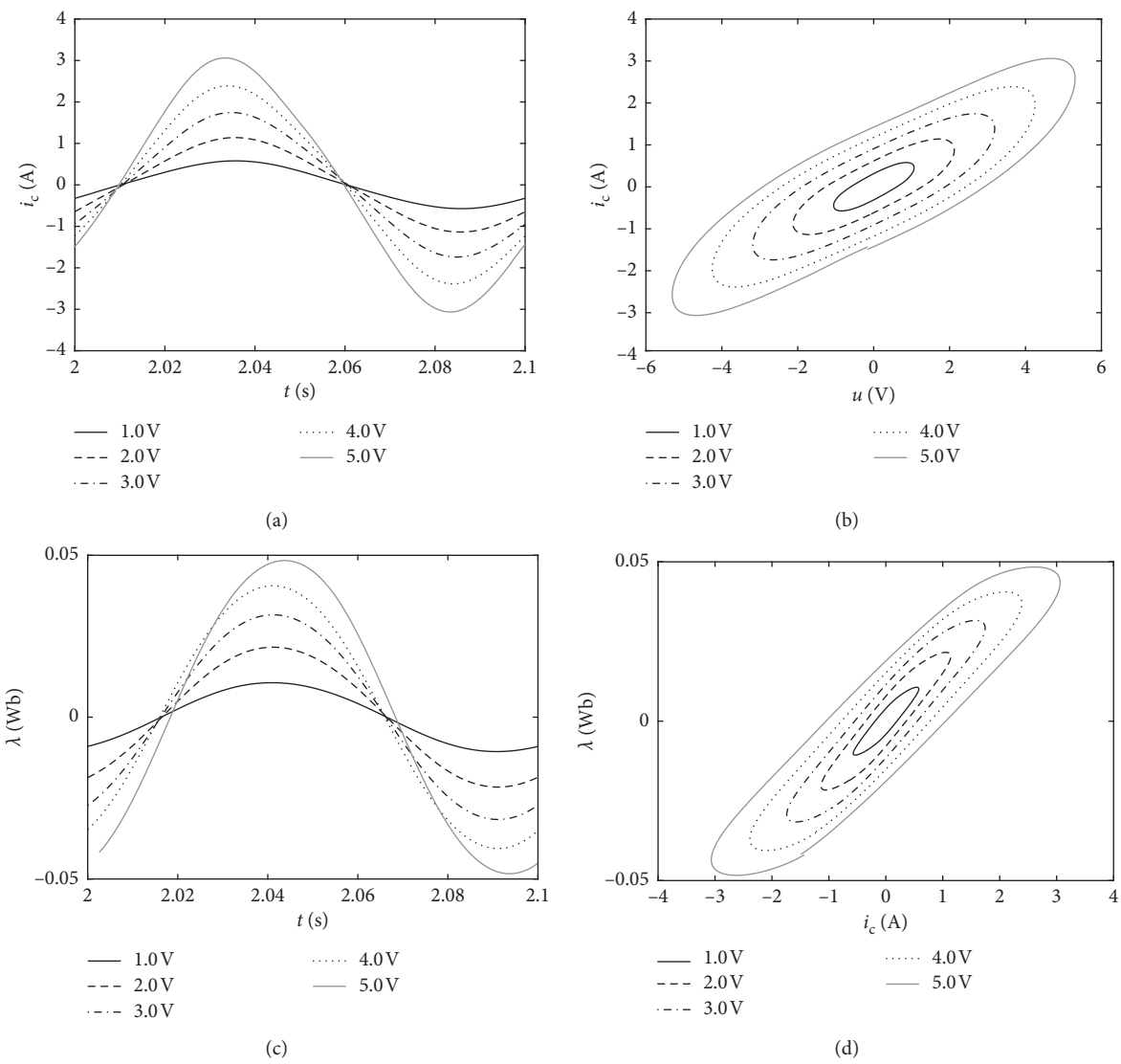

Figure 10: MRD1: sinusoidal input, $f = 10$ Hz. (a) i_c vs t, (b) i_c vs u, (c) λ vs t, and (d) λ vs i_c.

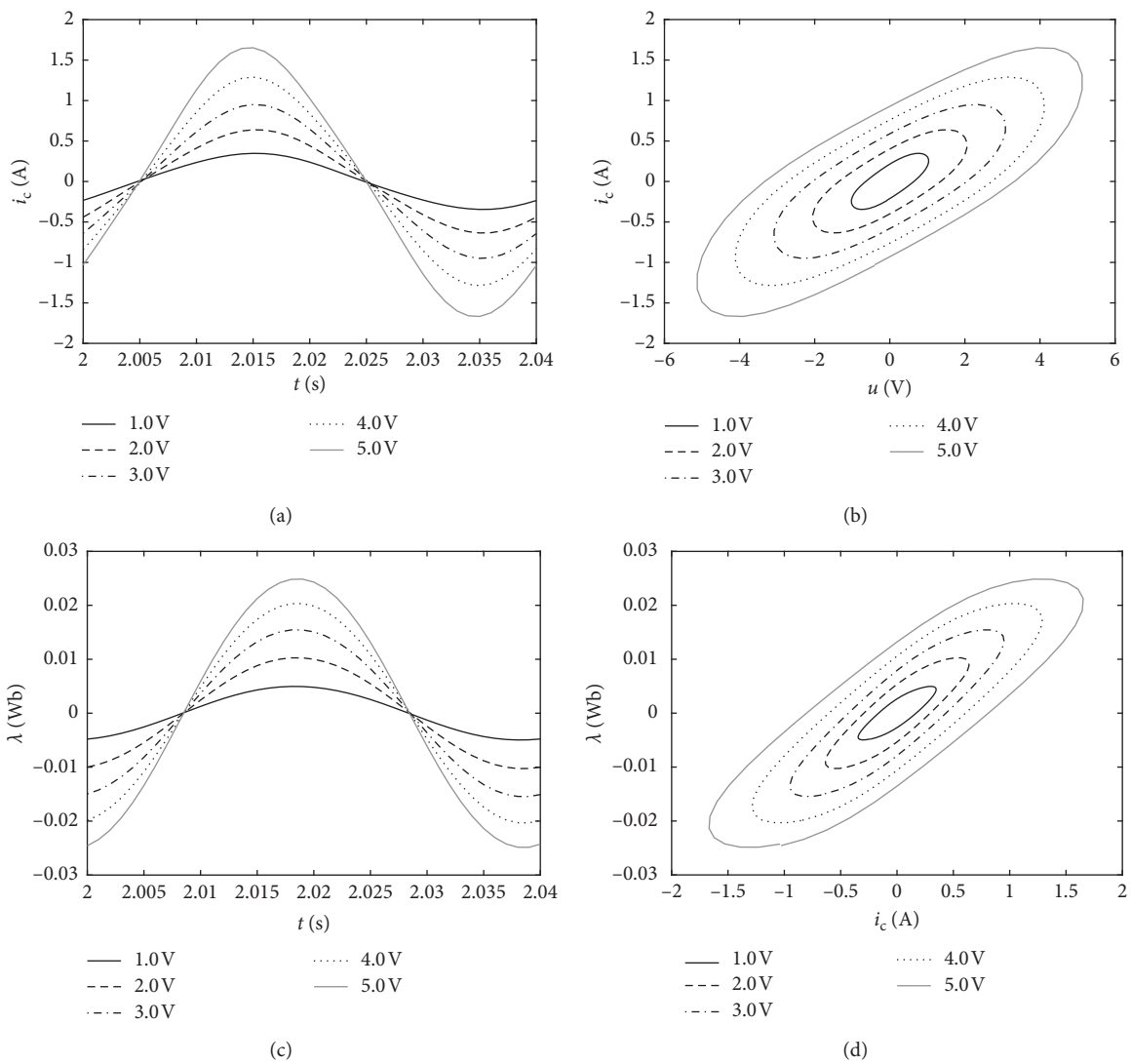

Figure 11: MRD1: sinusoidal input, $f = 25$ Hz. (a) i_c vs t, (b) i_c vs u, (c) λ vs t, and (d) λ vs i_c.

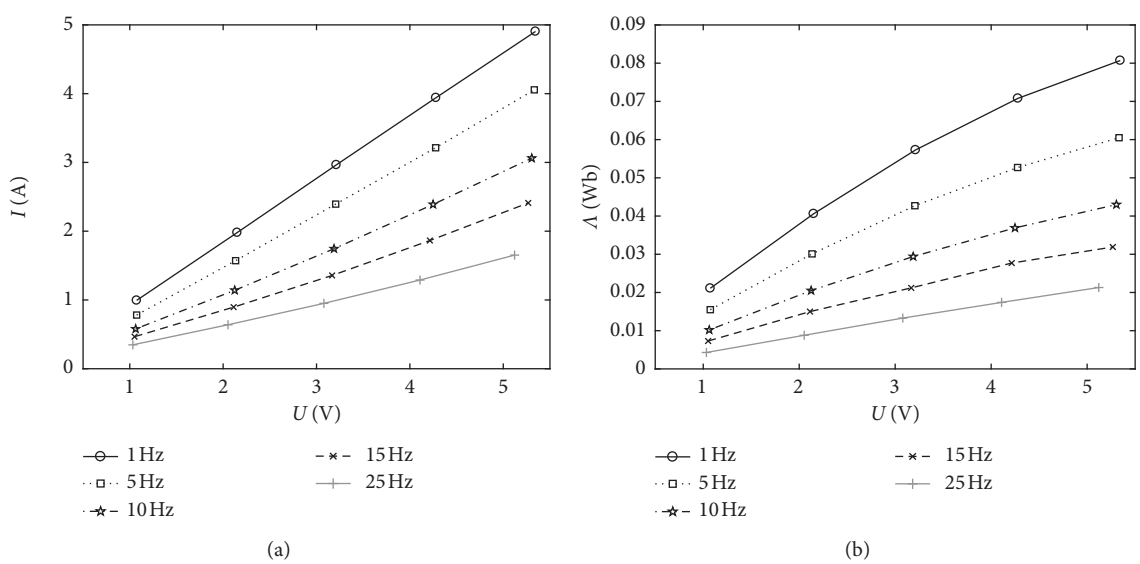

Figure 12: Continued.

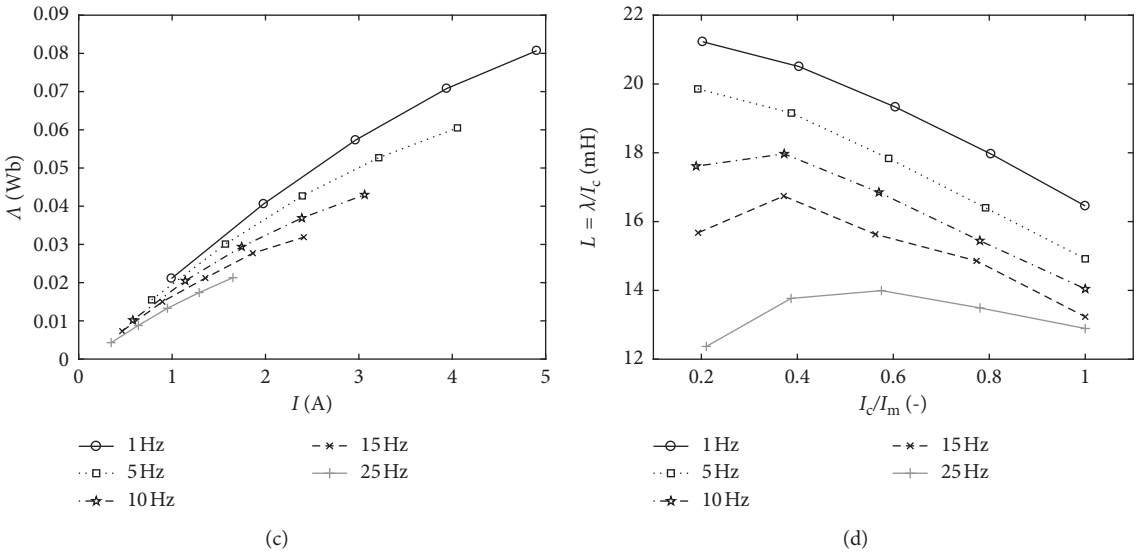

Figure 12: MRD1 characteristics. (a) I_c vs U, (b) Λ vs U, (c) Λ vs I_c, and (d) L vs I_c.

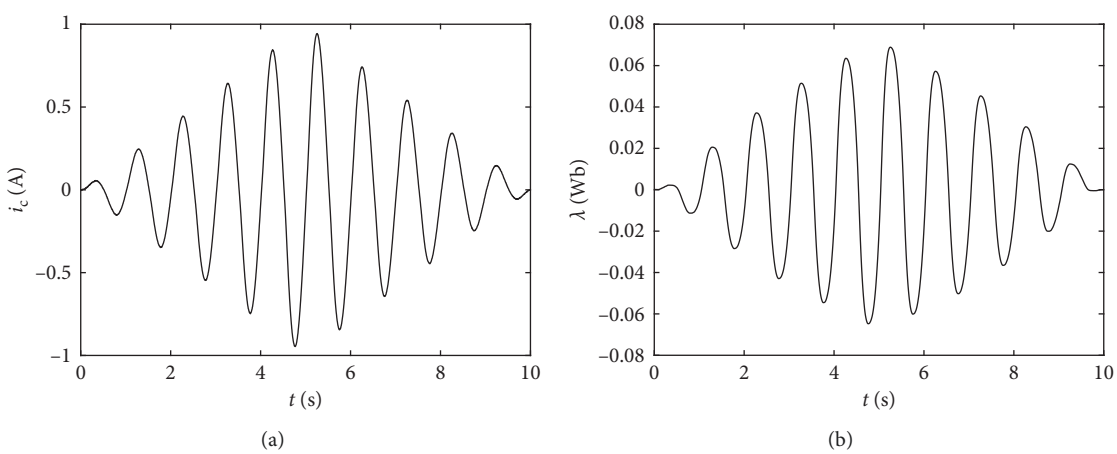

Figure 13: MRD2: time history of (a) current and (b) flux linkage.

5.2. Results: MRD2. In Figures 13–19, we illustrate the output performance of the small-stroke damper. Again, we first reveal the nonstationary amplitude test (Figures 13 and 14) results followed by the sinusoidal excitation response data shown in Figures 15–19. In this test scenario, the voltage input was varied to result in the peak current of 1 A at the frequency of $f = 1$ Hz.

The data show similar behaviour to that of MRD1 although it is of different magnitude. For example, the calculated inductance data show larger variation range of the parameter from approximately 40 mH to 90 mH (Figure 19(d)). That contrasts, for example, with the inductance data of the damper MRD1 for which the calculated variation range was from approximately 16 mH to 22 mH as revealed in Figure 12(d). Similarly to MRD1, the flux versus current relationship resembles that of magnetic hysteresis.

5.3. Results: MRD3. Finally, in Figures 20–26, we show the test output of the rotary damper. In a manner similar to MRD2, we varied the input voltage to result in the peak current of 1 A. This damper produces the highest flux linkage output of the examined dampers ($\Lambda = 0.3$ Wb) (Figure 26(c)). It also exhibits the largest coil resistance and the inductance (reaching 400 mH) as shown in Figure 26(d). As seen in Figure 26, the relationship between current and flux linkage is almost linear for smaller currents up to 0.4–0.5 A. The hysteresis shape as seen, for example, in Figure 22 resembles closely the MRD2's characteristics.

6. Summary

In this paper, we showed and analyzed the experimental results involving three commercial MR dampers. Two dampers were flow-mode devices, and the third one was a shear-mode brake. The research objective was to reproduce the magnetic hysteretic behaviour of these dampers by investigating the flux versus current relationship. As demonstrated through the response time data, the

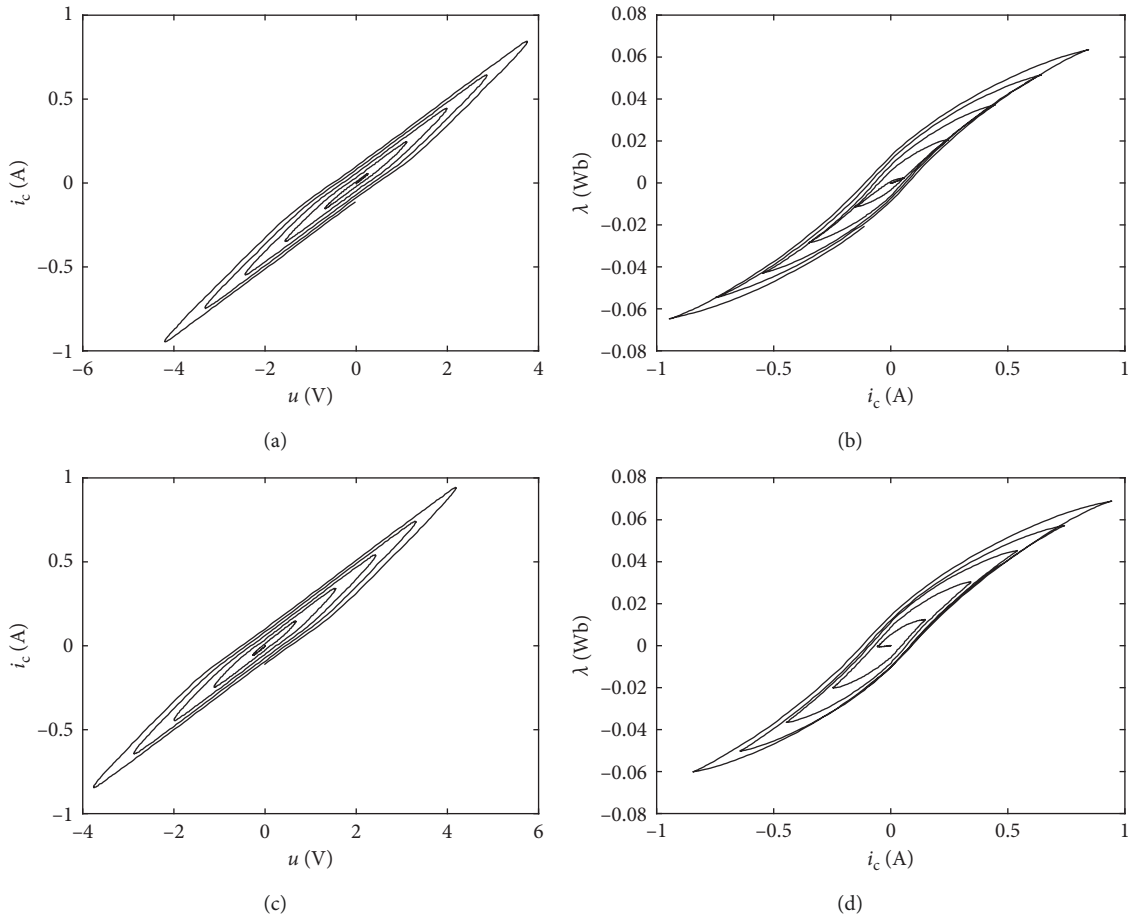

Figure 14: MRD2: (a, c) current versus voltage and (b, d) flux linkage versus current plots.

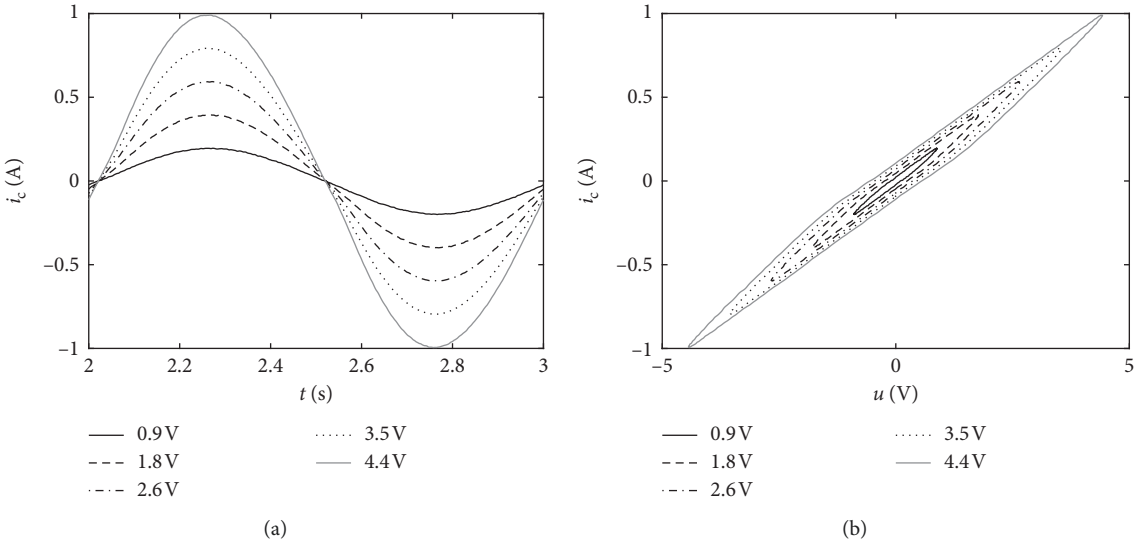

Figure 15: Continued.

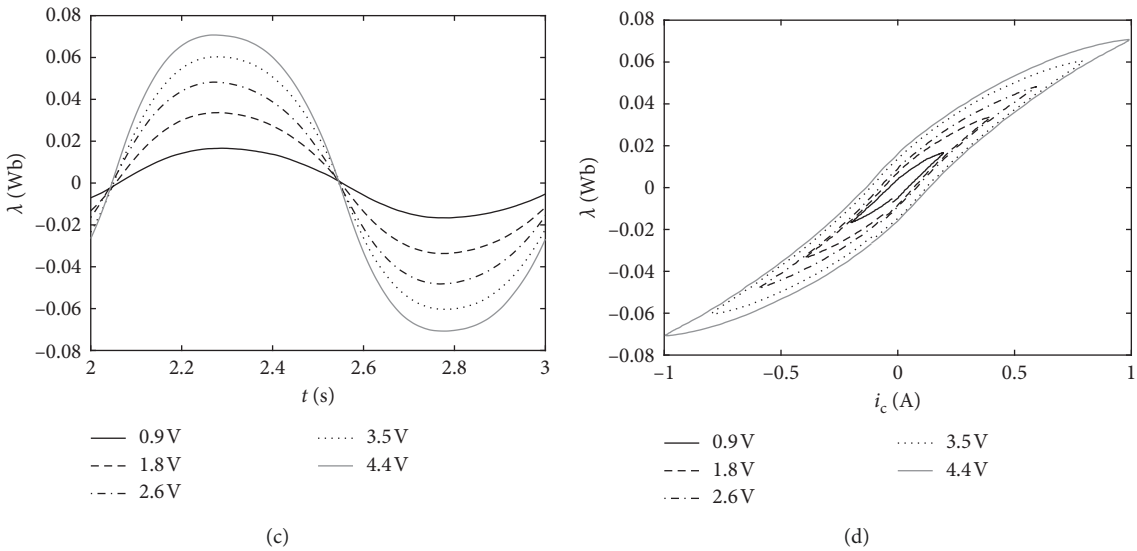

Figure 15: MRD2: sinusoidal input, $f = 1$ Hz. (a) i_c vs t, (b) i_c vs u, (c) λ vs t, and (d) λ vs i_c.

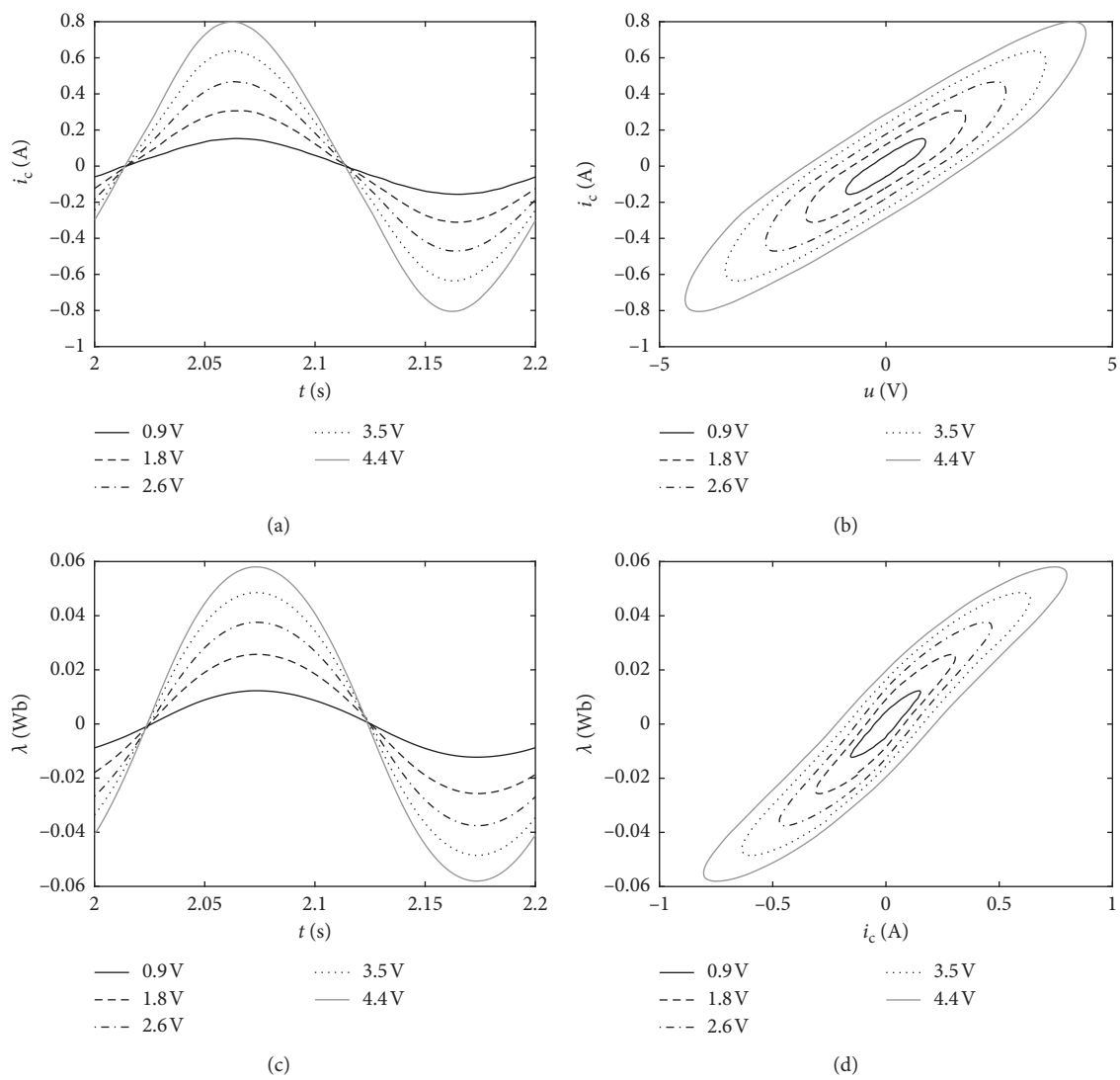

Figure 16: MRD2: sinusoidal input, $f = 5$ Hz. (a) i_c vs t, (b) i_c vs u, (c) λ vs t, and (d) λ vs i_c.

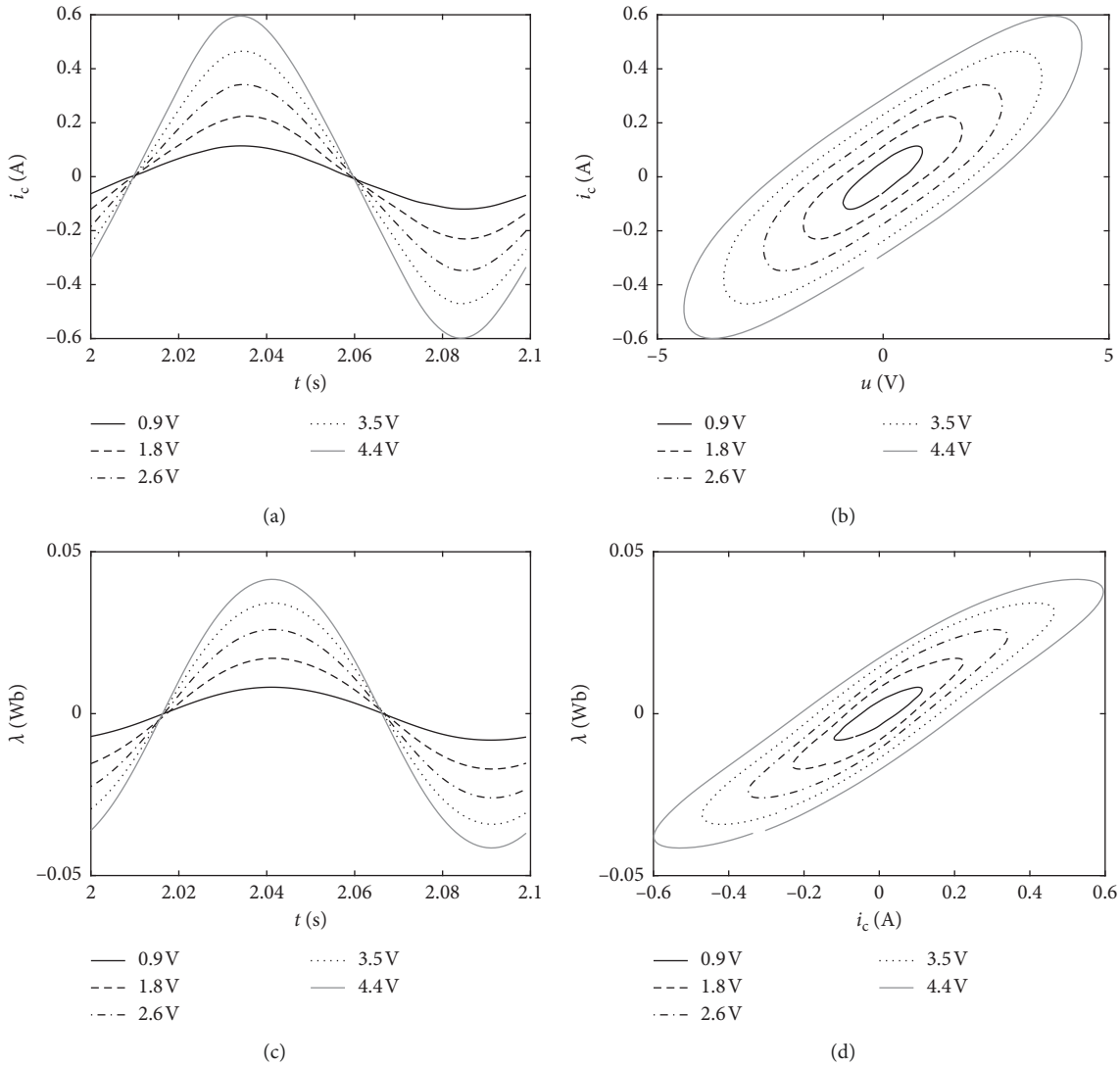

Figure 17: MRD2: sinusoidal input, $f = 10$ Hz. (a) i_c vs t, (b) i_c vs u, (c) λ vs t, and (d) λ vs i_c.

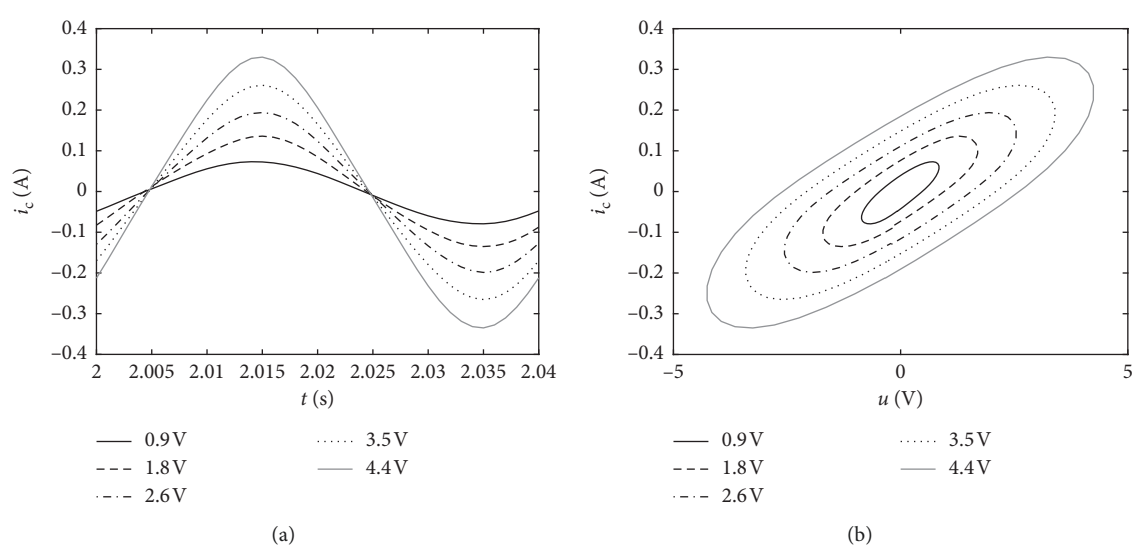

Figure 18: Continued.

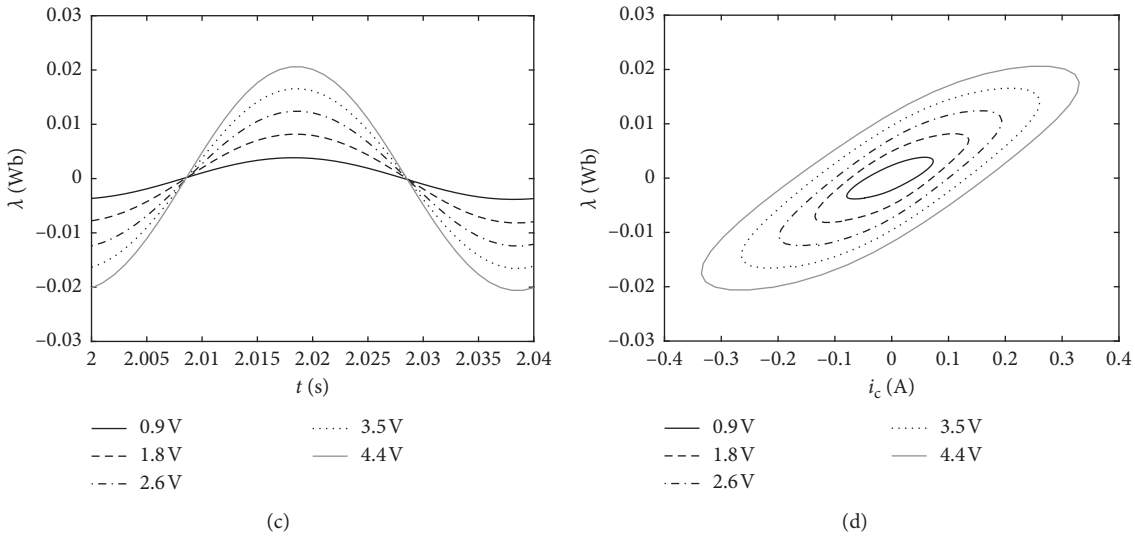

Figure 18: MRD2: sinusoidal input, f = 25 Hz. (a) i_c vs t, (b) i_c vs u, (c) λ vs t, and (d) λ vs i_c.

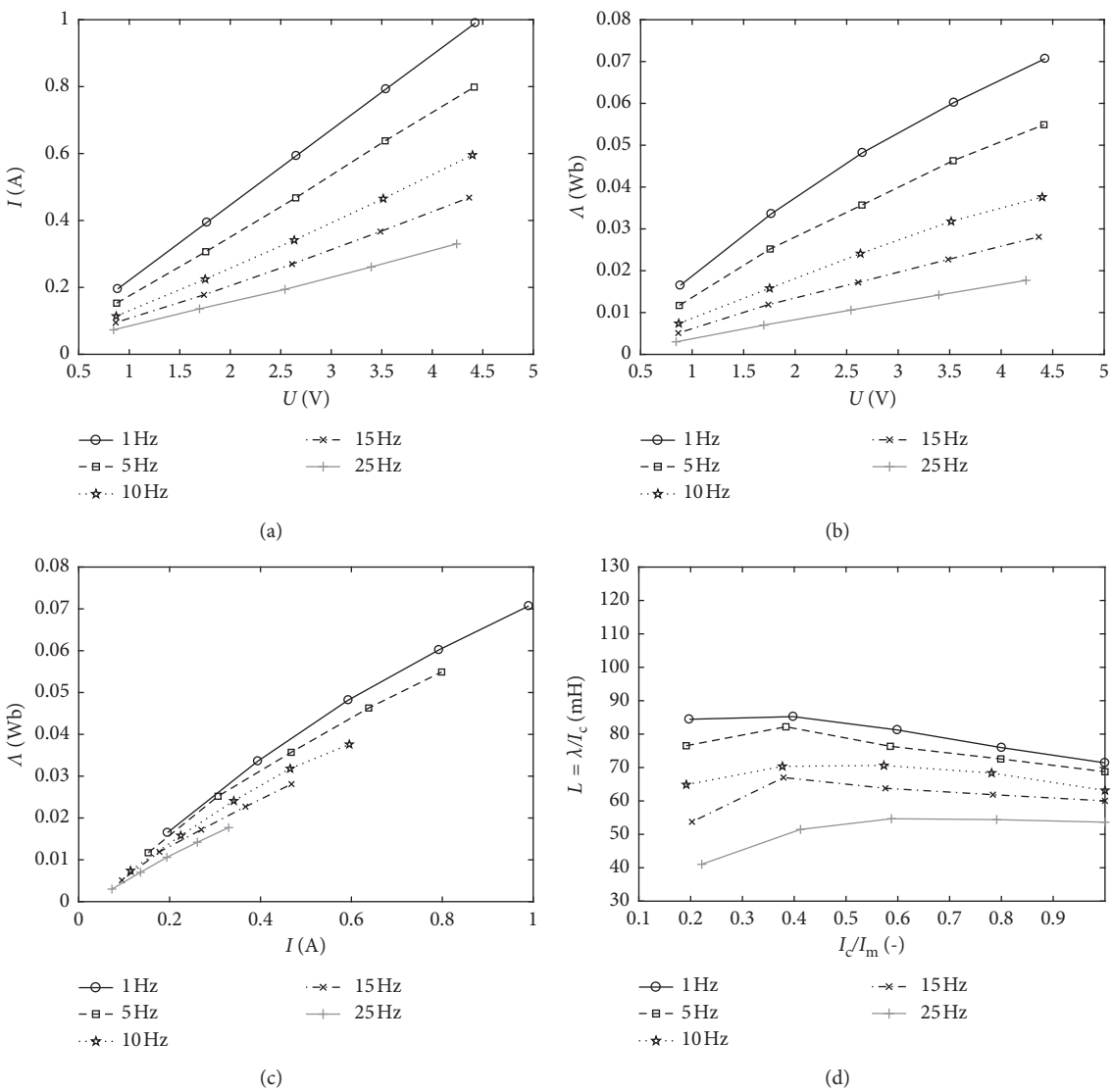

Figure 19: MRD2 characteristics. (a) I_c vs U, (b) Λ vs U, (c) Λ vs I_c, and (d) L vs I_c.

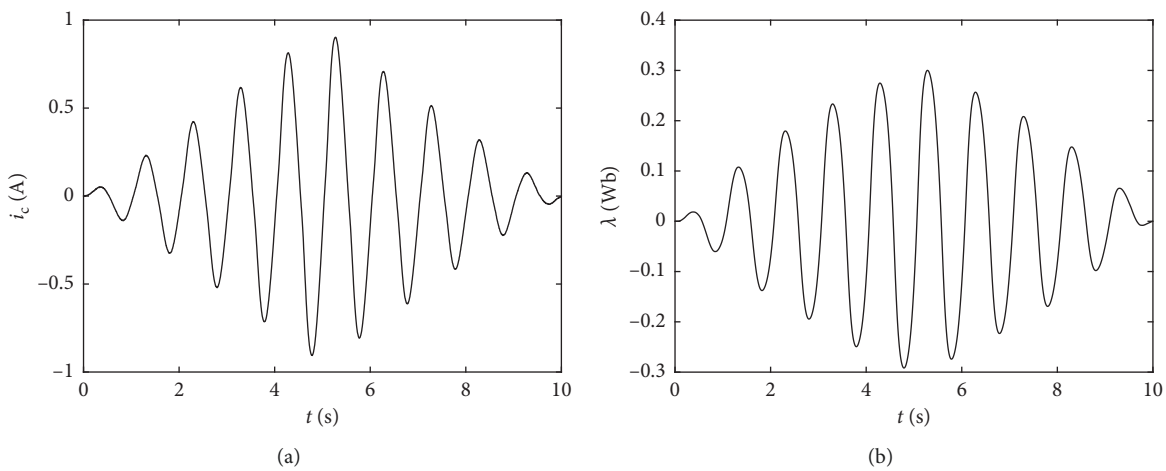

Figure 20: MRD3: time history of (a) current and (b) flux linkage.

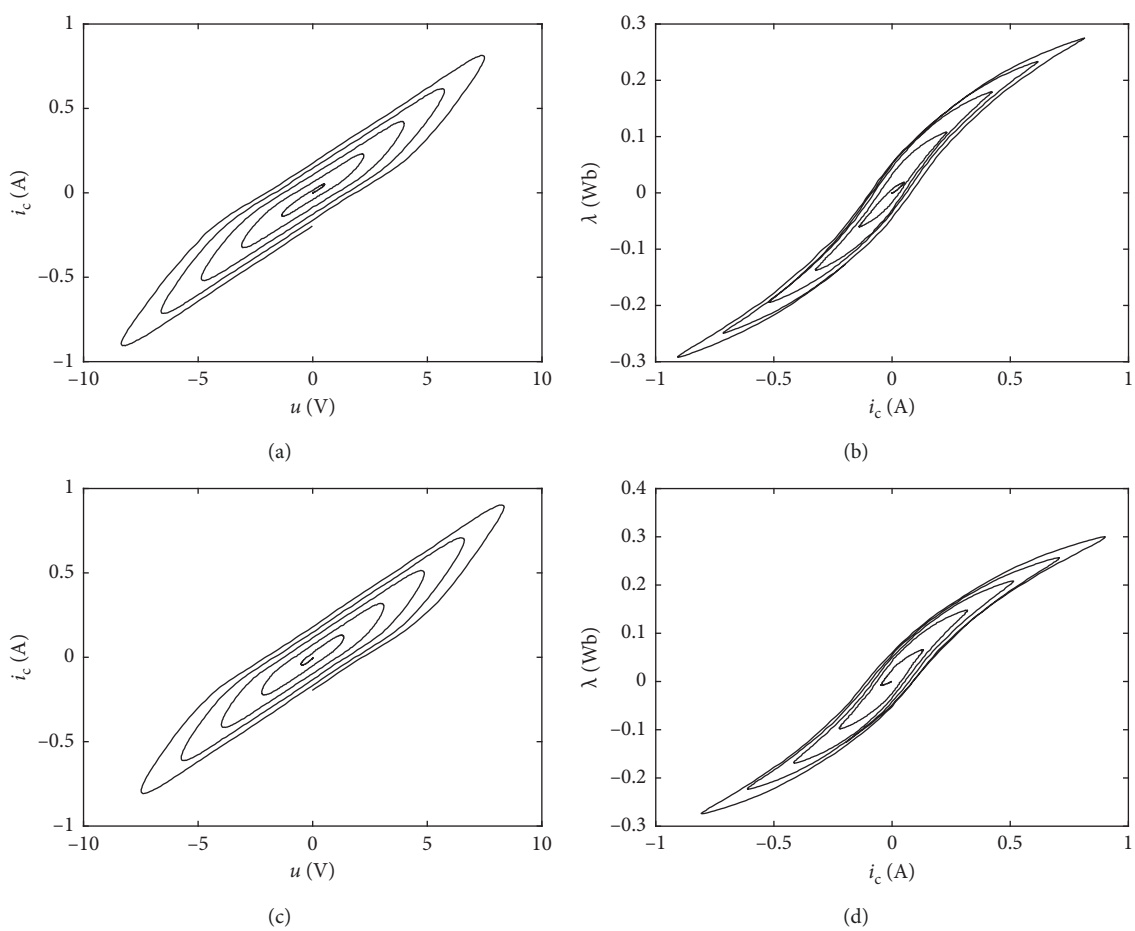

Figure 21: MRD3: current versus voltage and flux linkage versus current plots. (a) i_c vs t, (b) i_c vs u, (c) λ vs t, and (d) λ vs i_c.

performance range of the examined dampers was wide. Internal details of the dampers (core/coil geometry, control gap size) were unknown. Therefore, only the extraction of flux linkage data from the measurements was possible.

The flux was estimated using a sensorless approach which relies on voltage and current measurements of the control circuit followed by offline integration. The technique can be adapted to online measurements provided a simultaneous coil resistance estimate is determined. Also, at the present stage, the flux estimation approach is rid of a drift compensation mechanism. For the online version, a mutation of the algorithm with drift compensation (closed loop correction) needs to be developed.

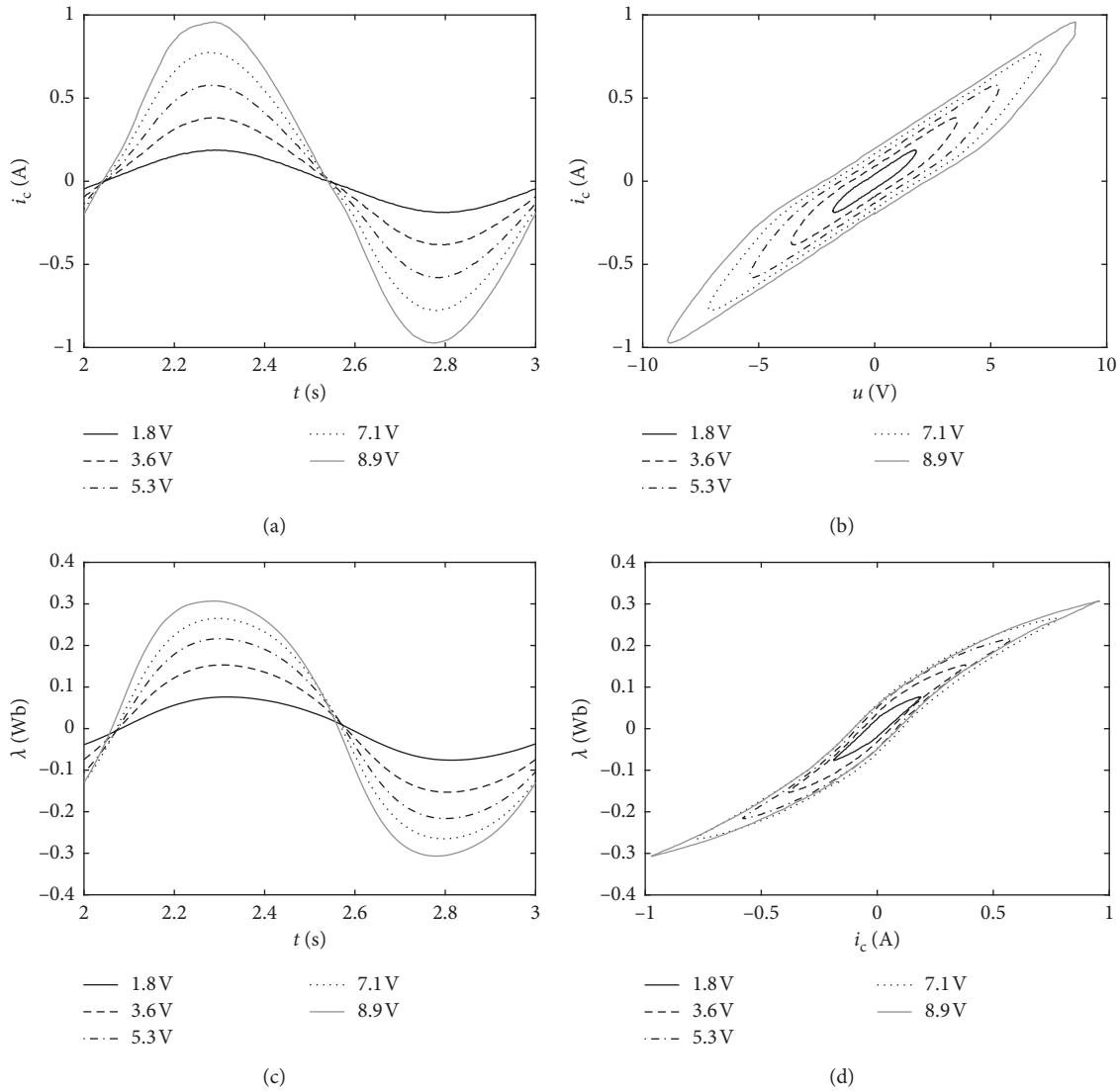

Figure 22: MRD3: sinusoidal input, $f = 1$ Hz. (a) i_c vs t, (b) i_c vs u, (c) λ vs t, and (d) λ vs i_c.

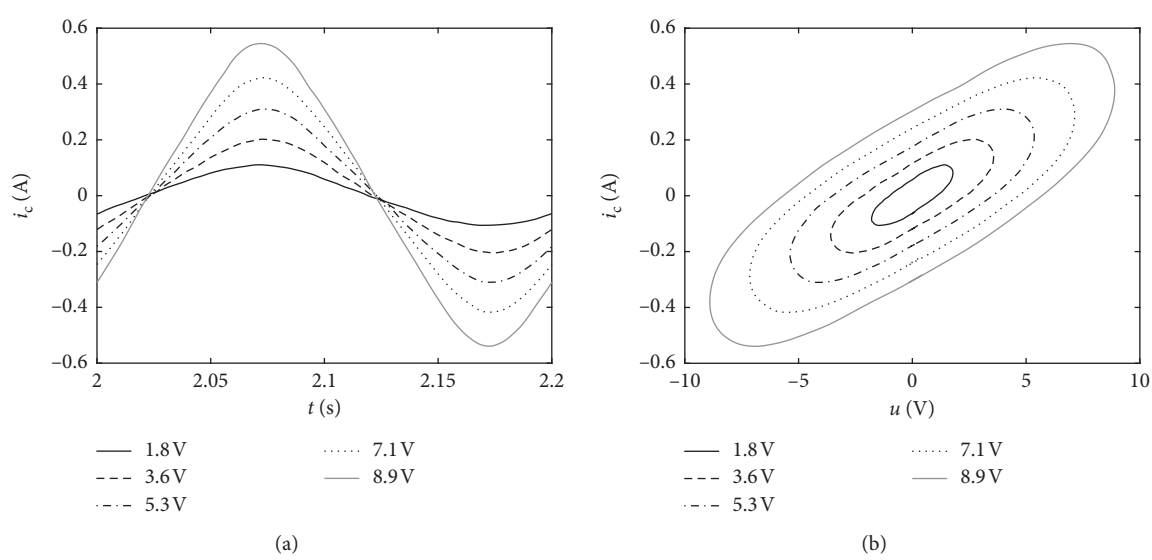

Figure 23: Continued.

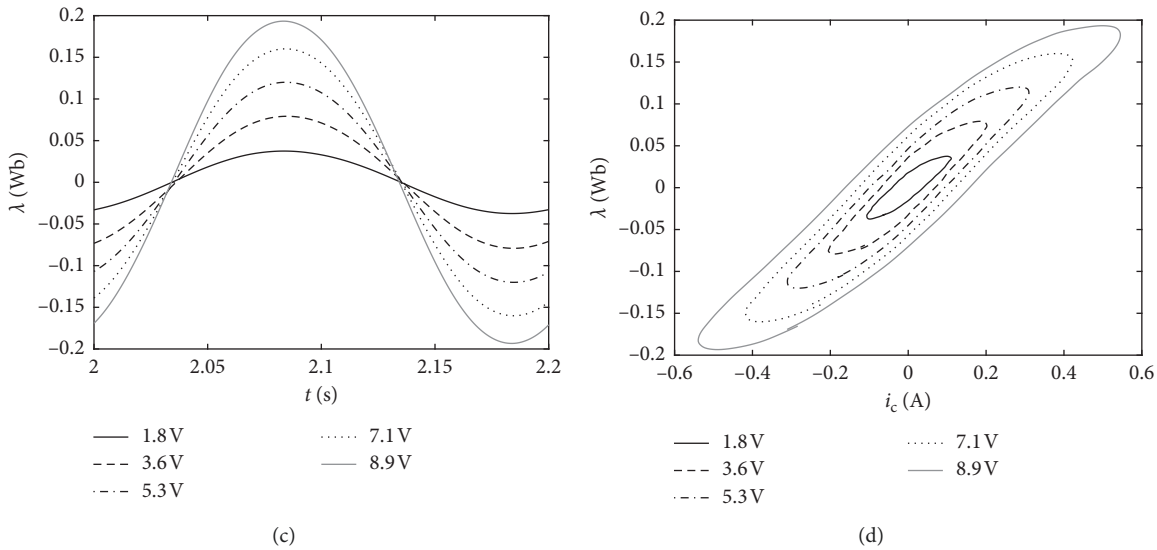

Figure 23: MRD3: sinusoidal input, f = 5 Hz. (a) i_c vs t, (b) i_c vs u, (c) λ vs t, and (d) λ vs i_c.

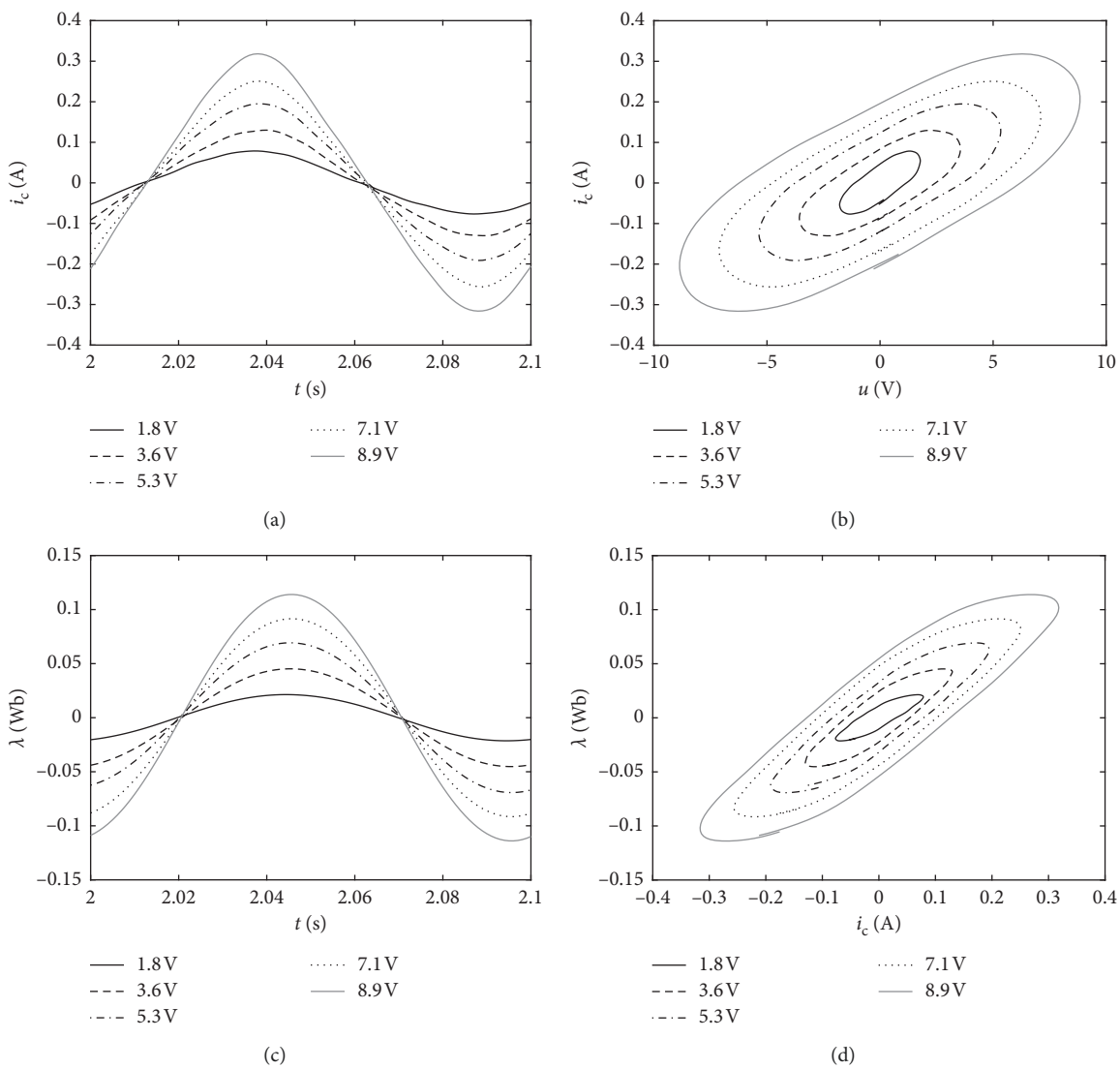

Figure 24: MRD3: sinusoidal input, f = 10 Hz. (a) i_c vs t, (b) i_c vs u, (c) λ vs t, and (d) λ vs i_c.

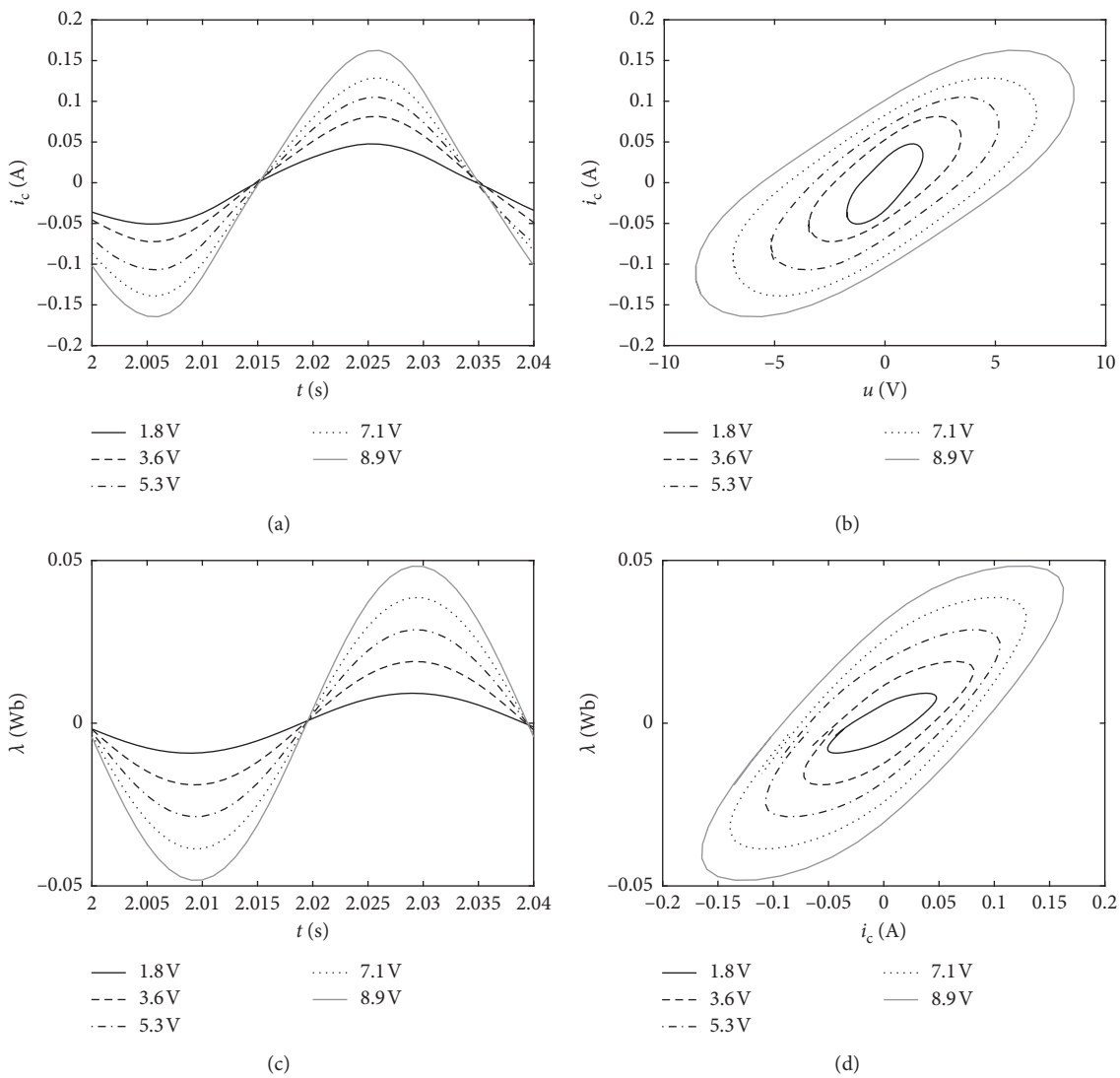

Figure 25: MRD3: sinusoidal input, f = 25 Hz. (a) i_c vs t, (b) i_c vs u, (c) λ vs t, and (d) λ vs i_c.

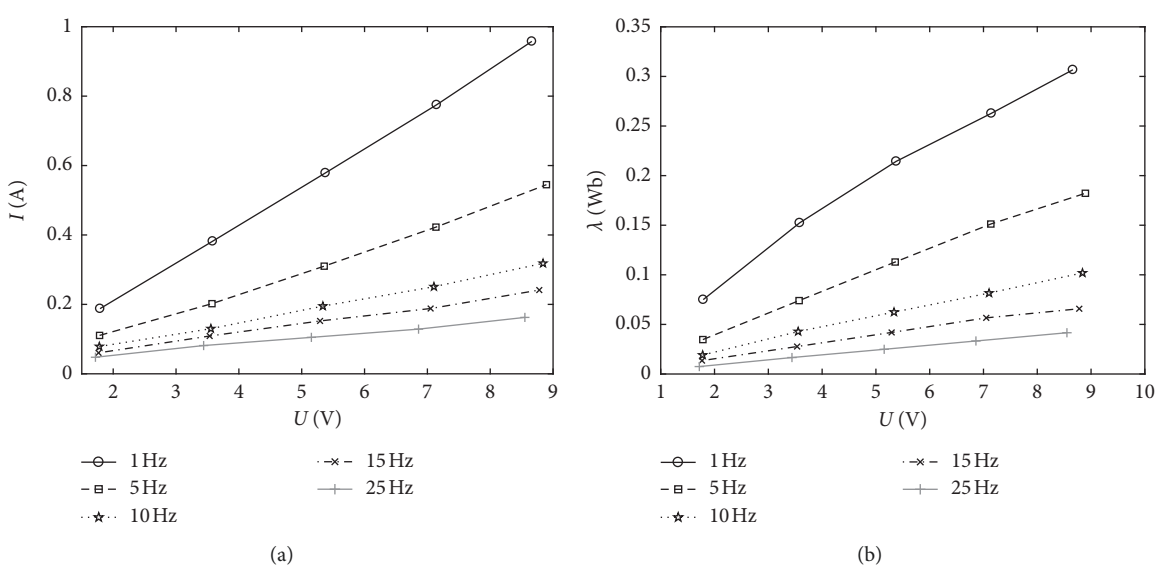

Figure 26: Continued.

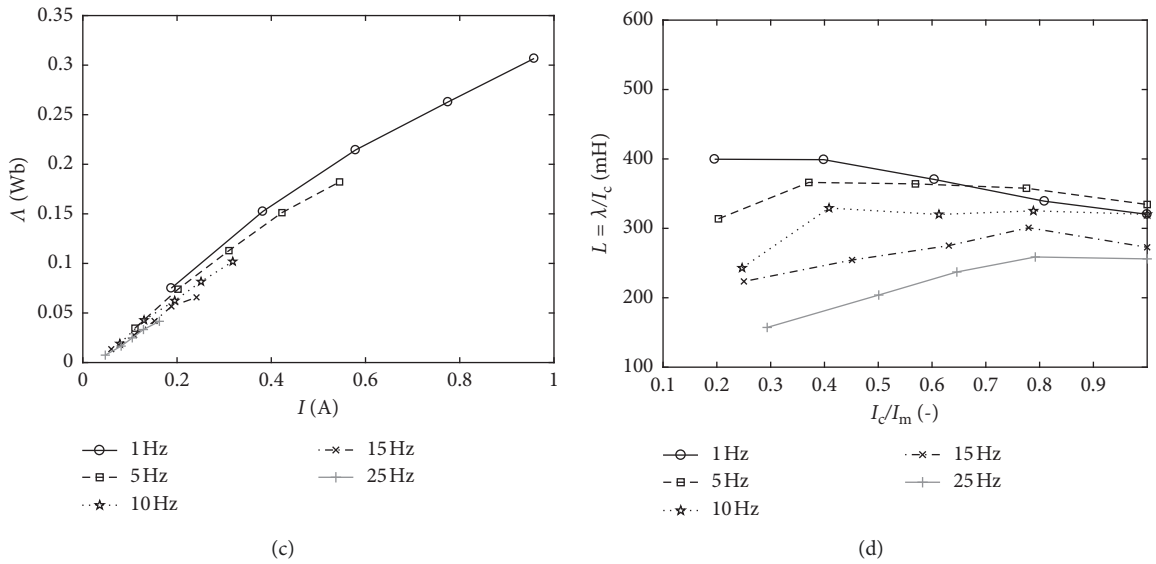

Figure 26: MRD3 characteristics. (a) I_c vs U, (b) Λ vs U, (c) Λ vs I_c, and (d) L vs I_c.

The study concerned the dampers' response to sinusoidal excitations. The hysteretic behaviour which we recorded and analyzed was shown to be a complex function of both the frequency and the input current. The shape of the (averaged) flux linkage versus current curve $\lambda - i$ resembles that of magnetic hysteresis. The $\lambda - i$ loop shape and width change with the current applied and the input frequency. Apparently, at low frequencies and high current levels, saturation effects were captured. As the input voltage frequency increased, the coil impedance was upgraded which resulted in lower peak amplitudes of the measured current and flux linkage, respectively. The obtained data also show that the flux linkage in the examined structures is affected by eddy currents which also explains the calculated coil inductance drop with the frequency (and the current). Additionally, the inductance deterioration at low currents may have been caused by measurement noise further augmented by the flux integrator.

The results of this series of experiments may be also applicable to self-powered vibration isolation systems with energy harvesters which feature a direct connection between the harvester and the MR damper [36]. Recently, this technique was also applied to squeeze-mode MR dampers [37].

The procedure provides means for separating the magnetic hysteresis from other sources of hysteresis in MR dampers so that the specific effects can be analyzed independently. It provides the information for developing more precise damper models and designing effective control algorithms. For example, the study shows that the nonlinearity due to magnetic hysteresis needs to be analyzed separately from the damper's hysteresis due to MR fluid's compressibility for optimum results. It reveals the dependency of the magnetic circuit's characteristics on the current magnitude and frequency of the excitation. Finally, improving the sensorless technique and extending it to other scenarios will be then explored in future, too.

Data Availability

The datasets generated during and/or analyzed during the current study are available from the corresponding author on request.

Conflicts of Interest

The authors declare that there are no conflicts of interest regarding the publication of this paper.

Acknowledgments

This work was supported by the AGH University of Science and Technology under the research program no. 11.11.130.958.

References

[1] J. Rabinow, "Magnetic fluid torque and force transmitting device," U.S. Patent No 2575360, 1951.

[2] P. N. Hopkins, J. D. Fehring, I. Lisenker et al., "Magnetorheological fluid damper," US Patent No. 6311810, 2003.

[3] J. Goldasz and S. Dzierzek, "Parametric study on the performance of automotive MR shock absorbers," *IOP Conference Series: Materials Science and Engineering*, vol. 148, no. 1, article 012004, 2016.

[4] J. Goldasz and A. A. Alexandridis, "Medium-and high-frequency analysis of magnetorheological fluid dampers," *Journal of Vibration and Control*, vol. 18, no. 14, pp. 2140–2148, 2012.

[5] J. De Vicente, G. Bossis, S. Lacis, and M. Guyot, "Permeability measurements in cobalt ferrite and carbonyl iron powders and suspensions," *Journal of Magnetism and Magnetic Materials*, vol. 251, no. 1, pp. 100–108, 1986.

[6] B. K. Bose, "An adaptive hysteresis-band current control technique of a voltage-fed PWM inverter for machine drive system," *IEEE Transactions on Industrial Electronics*, vol. 37, no. 5, pp. 402–408, 1998.

[7] I. D. Mayergoyz, G. Friedman, and C. Salling, "Comparison of the classical and generalized Preisach hysteresis models with experiments," *IEEE Transactions on Magnetics*, vol. 25, no. 5, pp. 3925–3927, 1989.

[8] D. C. Jiles and D. L. Atherton, "Theory of ferromagnetic hysteresis," *Journal of Applied Physics*, vol. 55, no. 6, pp. 2115–2120, 1984.

[9] D. C. Jiles, J. B. Thoelke, and M. K. Devine, "Numerical determination of hysteresis parameters for the modeling of magnetic properties using the theory of ferromagnetic hysteresis," *IEEE Transactions on Magnetics*, vol. 28, no. 1, pp. 27–35, 1992.

[10] A. Ramesh, D. C. Jiles, and J. M. Roderick, "A model of anisotropic anhysteretic magnetization," *IEEE Transactions on Magnetics*, vol. 32, no. 5, p. 4234, 1996.

[11] A. Raghunathan, Y. Melikhov, J. E. Snyder, and D. C. Jiles, "Modeling the temperature dependence of hysteresis based on Jiles-Atherton theory," *IEEE Transactions on Magnetics*, vol. 45, no. 10, pp. 3954–3957, 2009.

[12] J. Szczyglowski, "Influence of eddy currents on magnetic hysteresis loops in soft magnetic materials," *Journal of Magnetism and Magnetic Materials*, vol. 223, no. 1, pp. 97–102, 2001.

[13] B. D. Coleman and M. L. Hodgdon, "A constitutive relation for rate-independent hysteresis in ferro-magnetically soft materials," *International Journal of Engineering Science*, vol. 24, no. 6, pp. 897–919, 1986.

[14] J. Tellinen, "A simple scalar model for magnetic hysteresis," *IEEE Transactions on Magnetics*, vol. 34, no. 4, pp. 2200–2206, 1998.

[15] D. H. Wang and W. H. Liao, "Magnetorheological fluid dampers: a review of parametric modelling," *Smart Materials and Structures*, vol. 20, no. 2, article 023001, 2011.

[16] B. F. Spencer, S. J. Dyke, M. K. Sain, and J. D. Carlson, "Phenomenological model for magnetorheological dampers," *Journal of Engineering Mechanics*, vol. 123, no. 3, pp. 230–238, 1997.

[17] G. Yang, B. F. Spencer, H. J. Jung, and J. D. Carlson, "Dynamic modeling of large-scale magnetorheological damper systems for civil engineering applications," *Journal of Engineering Mechanics*, vol. 130, no. 9, pp. 1107–1114, 2004.

[18] Y. M. Han, S. B. Choi, and N. M. Wereley, "Hysteretic behavior of magnetorheological fluid and identification using Preisach model," *Journal of Intelligent Material Systems and Structures*, vol. 18, no. 9, pp. 973–981, 2007.

[19] S. B. Choi and Y. M. Han, "Hysteretic behavior of a magnetorheological fluid: experimental identification," *Acta Mechanica*, vol. 180, no. 1, pp. 37–47, 2003.

[20] P. Yadmellat and M. R. Kermani, "Output torque modeling of a magnetorheological based actuator," in *Proceedings of 18th World 18th IFAC World Congress*, vol. 18, pp. 1052–1057, Milano, Italy, September 2011.

[21] J. An and D. S. Kwon, "Modeling of a magnetorheological actuator including magnetic hysteresis," *Journal of Intelligent Material Systems and Structures*, vol. 14, no. 9, pp. 541–550, 2003.

[22] P. Yadmellat and M. R. Kermani, "Adaptive hysteresis compensation for a magnetorheological robot actuator," in *Proceedings of 2013 IEEE/RSJ International Conference on Intelligent Robots and Systems*, pp. 4900–4905, Tokyo, Japan, November 2013.

[23] P. Yadmellat and M. R. Kermani, "Adaptive modeling of a magnetorheological clutch," *IEEE/ASME Transactions on Mechatronics*, vol. 19, no. 5, pp. 1716–1723, 2014.

[24] J. Zheng, Y. Li, Z. Li, and J. Wang, "Transient multi-physics analysis of a magnetorheological shock absorber with the inverse Jiles-Atherton hysteresis model," *Smart Materials and Structures*, vol. 24, no. 10, article 105024, 2015.

[25] Lord Corp, *RD-8040 MR Damper. Technical Specification*, Lord Corp, Cary, NC, USA, 2016, http://www.lordmrstore.com.

[26] Lord Corp, *RD-2028 MR Brake. Technical Specification*, Lord Corp, Cary, NC, USA, 2016, http://www.lordmrstore.com.

[27] InTeCo, *RT-DAC 4 PCI Multi I/O Board. Technical Specification*, InTeCo, Austria, 2014, http://www.inteco.com.pl.

[28] T. W. Nehl, S. Gopalakrishnan, and F. Deng, "Direct flux control system for magnetic structures," US Patent Application No. US20070285195 A1, 2007.

[29] C. S. Namuduri, T. W. Nehl, A. M. Omekanda, and S. Gopalakrishnan, "Parameter estimation in an actuator," US Patent No. 9664159, 2017.

[30] S. Gopalakrishnan, T. W. Nehl, C. S. Namuduri, and A. M. Omekanda, "Magnetic force based actuator control," US Patent Application No. US 2015/0267666 A1, 2015.

[31] T. W. Nehl, C. S. Namuduri, A. M. Omekanda, and S. Gopalakrishnan, "Actuator with integrated flux sensor," US Patent No. 9657699, 2017.

[32] B. Ufnalski, *Application of neural networks for the reproduction of both angular velocity of the rotor and the stator flux in a drive system with a squirrel cage motor*, Ph.D. thesis, Warsaw University of Technology, Warsaw, Poland, 2004.

[33] M. Hinkkanen and J. Luomi, "Modified integrator for voltage model flux estimation of induction motors," *IEEE Transactions on Industrial Electronics*, vol. 50, no. 4, pp. 818–820, 2003.

[34] M. Hinkkanen, *Flux estimators for speed-sensorless induction motor drives*, Ph.D. Thesis, Helsinki University of Technology, Helsinki, Finland, 2004.

[35] J. Hu and B. Wu, "New integration algorithms for estimating motor flux over a wide speed range," *IEEE Transactions on Power Electronics*, vol. 13, no. 5, pp. 969–977, 1998.

[36] B. Sapinski, "Energy-harvesting linear MR damper: prototyping and testing," *Smart Materials and Structures*, vol. 23, article 035021, 2014.

[37] B. Sapinski and J. Goldasz, "Reproducing the magnetic hysteretic behaviour of an MR squeeze-mode actuator," in *Proceedings of 2018 19th International Carpathian Control Conference (ICCC)*, pp. 33–38, Szilvasvarad, Hungary, May 2018.